大阪公立大学
Osaka Metropolitan University
学術情報リポジトリ

Attitude Control of Small Satellites Using Single-Gimbal Control Moment Gyros

メタデータ	言語: eng 出版者: 公開日: 2010-07-26 キーワード (Ja): キーワード (En): 作成者: Kwon, Sangwon メールアドレス: 所属:
URL	https://doi.org/10.24729/00000034

Attitude Control of Small Satellites Using Single-Gimbal Control Moment Gyros

Sangwon Kwon

February 2010

Doctoral Thesis at Osaka Prefecture University

Attitude Control of Small Satellites Using Single-Gimbal Control Moment Gyros

Sangwon Kwon

February 2010

Doctoral Thesis at Osaka Prefecture University

Acknowledgments

First of all, I would like to express my gratitude to Professor Hiroshi Okubo, who is my supervisor of this research, for his great support, patient guidance, and constant encouragement throughout this research work. He taught me about the foundation for astronautical engineering and how to approach a research problem. I would also like to thank Professor Takeshi Manabe and Professor Masakatsu Chiba of Osaka Prefecture University for their reviewing this thesis.

I want to acknowledge Associate Professor Takashi Shimomura of Osaka Prefecture University for his useful suggestions, encouragement, and stimulating discussions with him. I also thank Assistant Professor Hiroshi Tokutake of Osaka Prefecture University for his useful comments and encouragement. I want to thank all students of our laboratory for their discussions and support.

I would like as well as thank Associate Professor Tomoo Takeguchi of Osaka Sangyo University for getting me interested in control engineering when I used to be a student at Osaka Sangyo University. I would also like to thank Lecturer Minako Ohashi of Osaka Sangyo University for her useful support and comment.

Finally, my warmest appreciation goes to my mother Myoungsook Kim, my brother Sanggun Kwon and my friends. Without their moral support and encouragement, I could not have completed this thesis.

Contents

List of Tables

List of Figures

Chapter 1

Introduction

1.1 Research Background

The term " small satellite " refers to a satellite of mass 500 kg or less as presented in Table 1.1. Recently, many space missions have been using small satellites, as shown in Fig. 1.1, because small satellites are easier and faster to develop and thereby, provide increased launch opportunities. Some of these missions include tasks that required agile maneuvers.

Most of the early small satellites were gravity gradient stabilized, with magnetic torques, acting as a passive actuator. TUBSAT-A a mass of 35 kg and launched in 1991, used magnetic torquers. Despite their low torque, momentum wheels (MWs) and

Table 1.1: Satellite classification [21]

Group Name	**Wet Mass**	**Classification**
Large Satellites	> 1000 kg	
Medium Satellites	500 - 1000 kg	
Mini Satellites	100 - 500 kg	
Micro Satellites	10 - 100 kg	
Nano Satellites	1 - 10 kg	**Small Satellites**
Pico Satellites	0.1 - 1 kg	
Femto Satellites	< 0.1 kg	

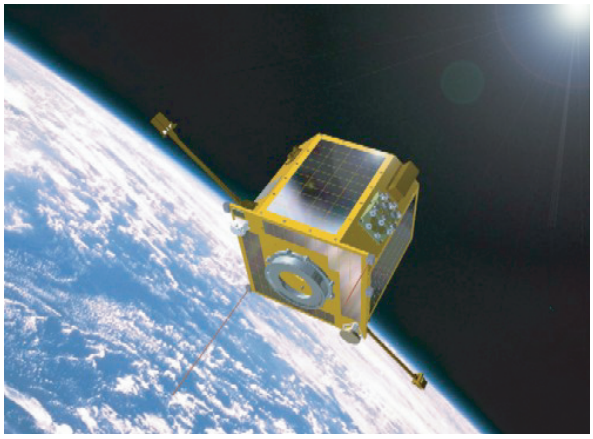

Figure 1.1: Small satellite: SOHLA-1

reaction wheels (RWs) were also used for the attitude control of small satellites. The first small satellite known to fly a momentum exchange device (MED) is TUBSAT-B, launched in 1994, designed by the Technical University of Berlin. SUNSAT with a mass of 60 kg and launched in 1999, was a micro satellite designed and built by Stellenbosch University. Figure 1.2 shows SUNSAT platform. SUNSAT used a gravity gradient boom, magnetorquers, and four RWs for maneuvers. UoSAT-12, an earth observation mini satellite designed by the University of Surrey with a mass of 320 kg launched in 1999 carried three RWs along with other actuators and thrusters.

In order endow small satellites with the ability to perform high-agile maneuvers, an attitude control system (ACS) using control moment gyros (CMGs) is proposed.

In the development of small satellites, the most severe constraints are limited power, mass, or capacity of various devices. Therefore, small-sized CMGs were developed. The installation of small CMGs in a small satellite can provide sufficient torque, angular momentum and slew rate, while not increasing the power consumption, mass, or volume of the satellite.

BILSAT-1, launched in 2003, was the first small satellite that used small CMGs to perform high agility maneuvers. The University of Surrey designed the small CMG used in the ACS of BILSAT-1. Figure 1.3 shows BILSAT-1 platform and CMG flight model.

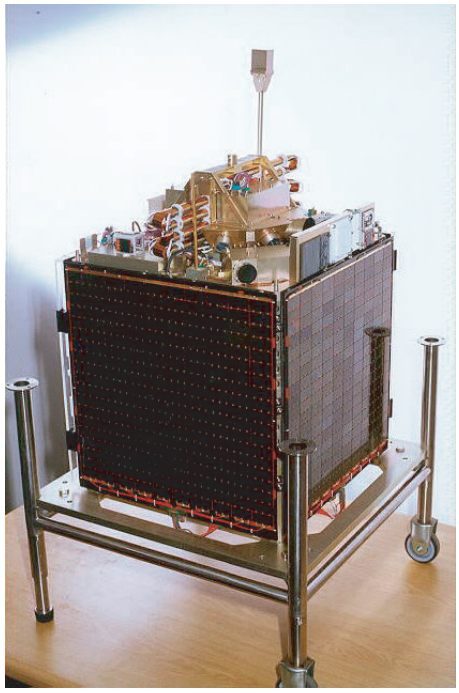

Figure 1.2: SUNSAT

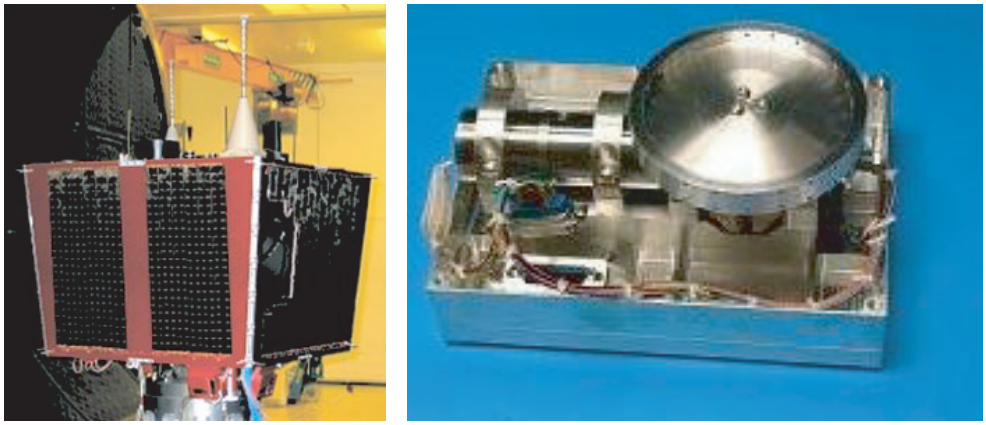

(a) BILSAT-1 (b) CMG system

Figure 1.3: BILSAT-a and CMG flight model

In the past, CMGs have been used for attitude control in large-sized satellites such as Skylab, MIR, and the International Space Station (ISS). However, attitude control with CMGs is also effective in small satellites, especially for high-speed or large-angle maneuvers.

This thesis describes the development of an ACS for small satellites using a small-sized CMG. The ACS was developed considering the following points:

- Singularity avoidance and fixed-star tracking attitude control
- Pointing attitude control of an under-actuated small satellite using only two SGCMGs
- Attitude control using SGCMGs via linear parameter-varying (LPV) control theory

In the following sections, the author describes the CMG system and describes the main topics.

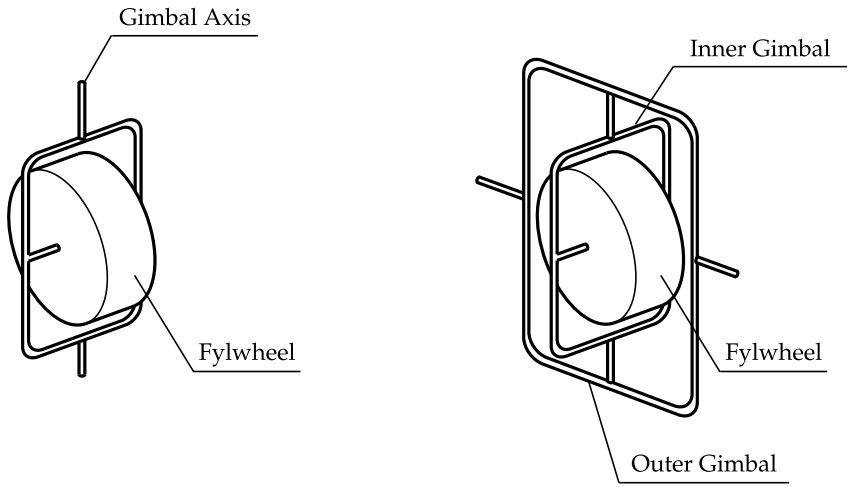

(a) Single-gimbal CMG (b) Double-gimbal CMG

Figure 1.4: Two types of CMG system

1.2 Control Moment Gyro

A CMG is a type of a MED used for attitude control of spacecrafts. It can generate substantially higher maximum output torque and store more angular momentum than reaction wheels. In addition, chemical fuels are not needed as thrusters.

CMG systems can be classified as single-gimbal CMG (SGCMG), double-gimbal CMG (DGCMG), as shown in Figure 1.4, and variable-speed CMG (VSCMG). An SGCMG has the advantages of having a simple mechanical structure and high torque amplification [11]. The flywheel of an SGCMG spins at a constant speed, and torquing of the gimbal results in a precessional, gyroscopic torque, that is orthogonal to both the spin and gimbal axes. However, an SGCMG system has the disadvantage of singularity. The singularity problem is described in the next section. A DGCMG has twice the degrees of freedom as that of an SGCMG, but its mechanical structure is complex. A VSCMG can generate a torque along any direction that lies on the plane perpendicular to the gimbal axis; this is because flywheel speed as well as gimbal rate of the VSCMG is provided as the control input. However, continuous variation of the flywheel speed can lead to vibration in the system; also its steering mechanism is complex.

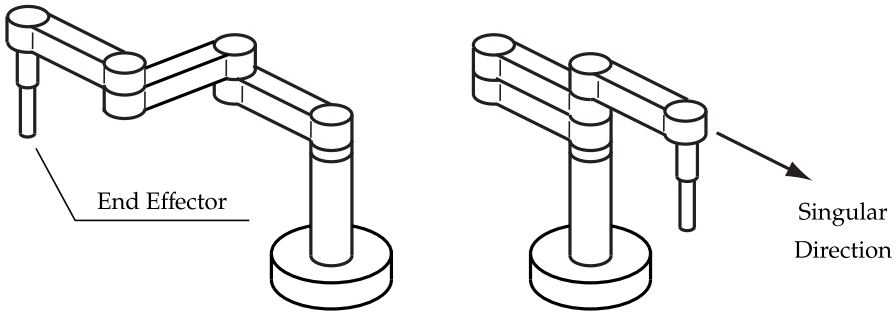

(a) Three link manipulator

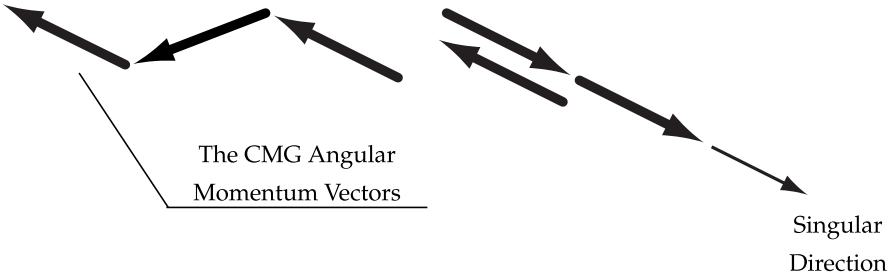

(b) Three SGCMG system

Figure 1.5: Example of singular state

In this thesis, an SGCMG system with a simple mechanical structure and negligible influence of vibration, is investigated. The use of SGCMGs (instead of VSCMGs with varying speeds) will decrease the vibration in small satellites, and thereby, lead to an increase in the pointing accuracy of the satellites.

1.3 Singularity of CMG System

With respect to attitude control using CMGs, the major problem is to avoid singularity. Singularity exists when there is some direction along which the array of CMGs cannot generate torque. This happens when the gimbal angles of CMGs are aligned in a specific arrangement. Figure 1.5 demonstrates the equivalence of the singularity problem for robotic manipulator and CMG system. In the case of manipulators, end-effector motion is impossible in the singular direction (Fig. 1.5 (a)), whereas for CMG system

case, torque cannot be generated along the singular direction (Fig. 1.5 (b)).

There are two types of singularities: external singularities and internal singularities. External singularities represent the maximum workspace of the total angular momentum of the CMG cluster, the so-called the angular momentum envelope. Because the external singularities are gimbal angles states that are reached at boundary of the angular momentum envelope, the CMG system cannot generate a torque beyond this envelope. Internal singularities exist inside the envelope (i.e., hyperbolic singularities and elliptic singularities).

Margulies et al. have established the mathematical analysis of an SGCMG cluster, and identified different types of singularities [11]. Kurokawa presented the characteristics of the singularities of SGCMGs from a geometric point of view [8]. Wie have been presented a mathematical nature of singularities and provided a visualization of several illustrative examples [24]. A mathematical analysis for the singularities of a VSCMG cluster is presented by Yoon et al. in Ref. [26].

The author briefly introduces a method developed by Margulies et al. for analyzing and visualizing the singularities of SGCMGs in Chapter 3.

1.4 Singularity Avoidance and Fixed-Star Tracking Attitude Control

Several techniques to avoid singularity, have been developed in the past. The so-called Singularity Robust (SR) steering law is developed by Nakamura and Hanafusa for robotic manipulators [14]. Wie applied the SR steering law to the singularity problem of CMG system and proposed the generalized SR steering logic [23]. These methods generate a torque error near the singular points to avoid singularities. On the other hand, there exists methods using null motion. Null motion is a motion of the gimbal angles without generating output torque. However, internal elliptic singularities cannot be escaped through null motion [2]. In addition, preferred gimbal angle [22], global search steering method [17], and constrained steering law [7] are proposed.

The author presents a simple method to avoid singularity in an SGCMG cluster by applying singular value decomposition (SVD). This steering method was proposed by Tani et al. [20, 16]. Using this method, a the direction vector perpendicular to

the singularities is obtained. In Chapter 3, the author considers fixed-star tracking attitude control of a spacecraft using four SGCMGs and applies the SVD method to avoid singularities. A numerical example of the fixed-star tracking control is provided to demonstrate the advantage of the proposed method over conventional SR steering method.

1.5 Pointing Attitude Control Using Two SGCMGs

The presence of singularities in the CMG system necessitates hardware redundancies (e.g., pyramid configuration for four SGCMGs). However, in the case of smaller-sized satellites with limited resources, hardware redundancies are not a suitable option. As a result, attitude control using a lesser number of CMGs have received considerable attention.

In the past, several studies on under-actuated spacecraft attitude control have been carried out. Typically, fewer than three actuators are used to provide three-axis control [6, 13].

Recently, Lappas et al. have addressed two parallel SGCMGs for the micro-satellite, BILSAT-1 [9]. Han et al. have studied the under-actuated attitude control problem of a spacecraft equipped with two parallel SGCMGs under the influence of external disturbances [5]. Marshall et al. have addressed the angular velocity stabilization of a spacecraft using a single VSCMG [12], while Yoon et al. [27] and Yamada et al. [25] have provided a control algorithm for line-of-sight control of a spacecraft via a single VSCMG.

Chapter 4 investigates the pointing control of a spacecraft using only two SGCMGs. Because the total angular momentum of a spacecraft is conserved in the inertial frame, the total CMG angular momentum is aligned with the total angular momentum of a spacecraft at a final state of rest. This imposes a restriction on the feasible orientations of the spacecraft's resting attitude. To solve this problem, the author proposes a two-step control strategy, i.e., nonlinear control based on the Lyapunov stability theory for all initial conditions at large followed by the linear quadratic regulator (LQR). The feasibility of the proposed two-step controller is verified by numerical simulation.

1.6 Attitude Control Using SGCMGs via Linear Parameter Varying Control Theory

In the past decades, several attempts were made to apply linear control techniques to nonlinear systems. Particularly, the gain-scheduled (GS) control based on the linear parameter-varying (LPV) approach has found applications in practical engineering design.

For a robot manipulator, a GS $\mathcal{H}_\infty$ controller, which places the closed-loop poles is presented in Ref. [28]. Gao. et al. proposed the LPV controller for changing depth of an underwater vehicle with velocity variation [4]. In the aerospace field, Shamma et al. presented a gain-scheduled design for a missile longitudinal autopilot [18]. Marcos et al. studied three LPV modeling techniques and presented their application to the Boeing 747 longitudinal motion [10].

For attitude control of a spacecraft using SGCMGs, a new control method based on the LPV control theory has been proposed in Chapter 5. Based on this theory, nonlinear dynamics of the spacecraft with SGCMGs were modeled as an LPV system and a GS controller was applied to this system. This GS controller consists of extreme controllers designed for each of the extremities of the convex hull that covers the operating region of the spacecraft modeled as an LPV system. In this chapter, the author describes a GS control algorithm based on the LPV control theory. The feasibility of the proposed control method is shown by a numerical simulation.

1.7 Outline of This Thesis

The organization of this thesis is as follows.

Chapter 2 describes the dynamics of rotational motion of a rigid spacecraft with an SGCMG cluster. It also describes the kinematics of rotational motion of a rigid spacecraft using several parameters to represent the attitude of a spacecraft.

Chapter 3 describes the singularities seen in a typical pyramid array of four SGCMGs. In addition, a simple singularity avoidance method using SVD is presented in this chapter. This method is applied to the fixed-stars tracking attitude control problem.

In Chapter 4, the author states the control objective for the pointing attitude control using two SGCMGs and proposes a control strategy which consists of two steps for

the control objective

For an attitude control problem of a spacecraft using SGCMGs, a new control method via LPV control theory is proposed in Chapter 5. Based on this theory, nonlinear dynamics of the spacecraft is described as an LPV system and an interesting GS controller is applied to this system.

Finally, Chapter 6 concludes this thesis, and provides directions for further study.

Chapter 2

System Model

2.1 Kinematics

The attitude of a rigid body is used to describe the orientation of one reference frame to another reference frame. In this thesis, two frames are defined as follows:

- Inertial Frame $\mathcal{F}_I$: An inertial frame which is represented by the orthonormal set of unit vectors $\hat{x}_I$, $\hat{y}_I$, and $\hat{z}_I$ is a non-rotating reference frame in fixed space.
- Body Frame $\mathcal{F}_B$: A body frame which is represented by the orthonormal set of unit vectors $\hat{x}_B$, $\hat{y}_B$, and $\hat{z}_B$ is fixed origin at a point on the spacecraft.

Many parameters can be used to represent the attitude orientations such as Euler angles, quaternions (so-called Euler parameters), and Modified Rodrigues Parameters (MRPs). The following subsections in this section introduce each parameters.

2.1.1 Euler Angles

Euler angles describe the attitude of a reference frame relative to the one another through three successive rotation angles about the sequentially displaced body fixed axes. The first rotation is about any axis. The second rotation is about either of the two axes not used for the first rotation. The third rotation is then about either of the two axes not used for the second rotation. Thus, Euler angles are useful for visualization because it is intuitively easier to understand.

Consider three successive rotation that describe the orientation of a reference frame

relative to the one another. The principal rotations are as follows:

$$R_x(\phi) = \begin{bmatrix} 1 & 0 & 0 \\ 0 & \cos\phi & \sin\phi \\ 0 & -\sin\phi & \cos\phi \end{bmatrix} \tag{2.1a}$$

$$R_y(\theta) = \begin{bmatrix} \cos\theta & 0 & -\sin\theta \\ 0 & 1 & 0 \\ \sin\theta & 0 & \cos\theta \end{bmatrix} \tag{2.1b}$$

$$R_z(\psi) = \begin{bmatrix} \cos\psi & \sin\psi & 0 \\ -\sin\psi & \cos\psi & 0 \\ 0 & 0 & 1 \end{bmatrix} \tag{2.1c}$$

Thus, a direction cosine matrix R_I^B from $\mathcal{F}_I$ to $\mathcal{F}_B$, in terms of the $x-y-z$ Euler angles is defined by

$$R_I^B = R_x(\phi)R_y(\theta)R_z(\psi) \tag{2.2}$$

2.1.2 Quaternions

The four element set of quaternions are defined by

$$q = [q_1,\ q_2,\ q_3]^T = \hat{\eta}\sin\frac{\phi}{2} \tag{2.3a}$$

$$q_4 = \cos\frac{\phi}{2} \tag{2.3b}$$

where $\hat{\eta} = [\eta_1,\ \eta_2,\ \eta_3]^T \in \mathbb{R}^3$ is the principal axis vector, ϕ is the rotation angle about principal axis. Note that the quaternions are not independent of each other, but constrained by the following relationship

$$q_1^2 + q_2^2 + q_3^2 + q_4^2 = 1 \tag{2.4}$$

Quaternions is widely used because it is singularity-free while it has minimum redundancy of one. The kinematic differential equation in terms of the quaternions is given by

$$\dot{q} = \frac{1}{2}(q_4\omega - \omega^{\times}q) \tag{2.5a}$$

$$\dot{q}_4 = -\frac{1}{2}\omega^T q \tag{2.5b}$$

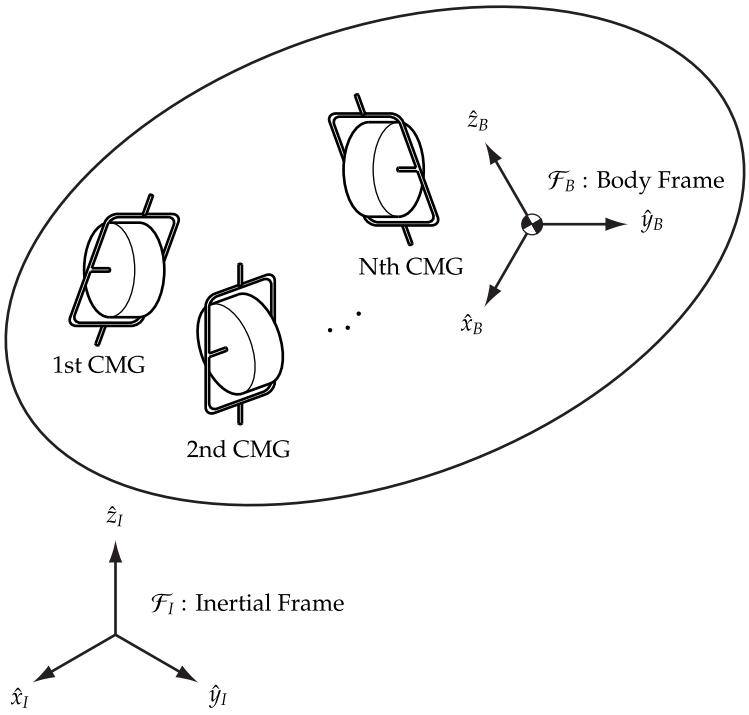

Figure 2.1: A rigid body with a cluster of N SGCMGs

2.1.3 Modified Rodrigues Parameters

The Modified Rodrigues Parameters (MRPs) are defined by using the principal axis η and the angle ϕ as follows:

$$\sigma = [\sigma_1,\ \sigma_2,\ \sigma_3]^T = \hat{\eta} \tan \frac{\phi}{4} \tag{2.6}$$

The MRPs have the advantage of being well defined for the whole range for rotations, i.e., $\phi \in [0, 2\pi)$, while they have no redundancy. The kinematic differential equation of the MRPs is given by

$$\dot{\sigma} = \frac{1}{2}\left(\frac{1}{2}(1 - \sigma^T\sigma)I_{3\times3} + \sigma^\times + \sigma^T\sigma\right)\omega \tag{2.7}$$

2.2 Dynamics

Consider a rigid spacecraft with a cluster of N SGCMGs, as shown in Fig. 2.1. The total angular momentum vector of a spacecraft with an SGCMG cluster, $H = [H_x,\ H_y,\ H_z]^T \in$

$\mathbb{R}^3$ can be expressed in the spacecraft body frame as

$$H = J\omega + h \tag{2.8}$$

where $J \in \mathbb{R}^{3\times3}$ is the inertia matrix of the spacecraft including an SGCMG cluster, $\omega = [\omega_x,\ \omega_y,\ \omega_z]^T \in \mathbb{R}^3$ is the angular velocity vector of the spacecraft, and $h = [h_x,\ h_y,\ h_z]^T \in \mathbb{R}^3$ is the CMG angular momentum vector expressed in the body frame. It is that h is the vector sum of each CMG angular momentum vectors as follows:

$$h = h_1 + \cdots + h_N = \sum_{i=1}^{N} h_i \tag{2.9}$$

where h_i is the individual angular momentum vector of the ith CMG.

Assuming that no external torque is applied to a spacecraft body, the equation of rotational motion of a rigid spacecraft equipped with an SGCMG cluster is given by

$$\dot{H} + \omega^{\times}H = 0 \tag{2.10}$$

For any vector $x = [x_x,\ x_y,\ x_z]^T \in \mathbb{R}^3$, $x^{\times} \in \mathbb{R}^{3\times3}$ denotes the skew-symmetric matrix, which is defined as

$$x^{\times} \triangleq \begin{bmatrix} 0 & -x_z & x_y \\ x_z & 0 & -x_x \\ -x_y & x_x & 0 \end{bmatrix} \tag{2.11}$$

By substituting Eq. (2.8) into Eq. (2.10), the following equation is obtained as

$$(J\dot{\omega} + \dot{h}) + \omega^{\times}(J\omega + h) = 0 \tag{2.12}$$

The CMG angular momentum vector h is a function of the gimbal angle vector $\delta = [\delta_1,\ \ldots,\ \delta_N]^T \in \mathbb{R}^N$ as follows:

$$h = h(\delta) \tag{2.13}$$

The time derivative of the CMG angular momentum vector is expressed as

$$\dot{h} = (\partial h/\partial\delta)\dot{\delta} \triangleq G(\delta)\dot{\delta} \tag{2.14}$$

where $G(\delta) \in \mathbb{R}^{3\times N}$ is the well known Jacobian matrix.

Thus, the complete equation of rotational motion of a spacecraft with an SGCMG cluster is given by

$$\dot{\omega} = -J^{-1}\omega^{\times}\left(J\omega + h(\delta)\right) - J^{-1}G(\delta)\dot{\delta} \tag{2.15}$$

where the gimbal rate $\dot{\delta}$ is the control input.

Chapter 3

Fixed-Star Tracking Attitude Control of Spacecraft Using SGCMGs

3.1 Dynamics of Spacecraft with an SGCMG Cluster

Equation (2.12) can be divided into the following two equations if the internal torque generated by CMGs is denoted as $\tau \in \mathbb{R}^3$:

$$J\dot{\omega} + \omega^{\times} J\omega = \tau \tag{3.1a}$$

$$\dot{h} + \omega^{\times} h = -\tau \tag{3.1b}$$

Thus the dynamic equation of motion of a spacecraft equipped with CMGs consists of the dynamics of the spacecraft (Eq. (3.1a)) and the dynamics of the CMG system (Eq. (3.1b)). The desired CMG angular momentum rate for generating the spacecraft control torque is given by

$$\dot{h} \triangleq T = -\tau - \omega^{\times} h \tag{3.2}$$

The CMG angular momentum vector $h = h(\delta)$ is a function of the gimbal angle vector $\delta \in \mathbb{R}^N$, then the time derivative of h is obtain as

$$\dot{h} = (\partial h/\partial \delta)\dot{\delta} \triangleq G\dot{\delta} \tag{3.3}$$

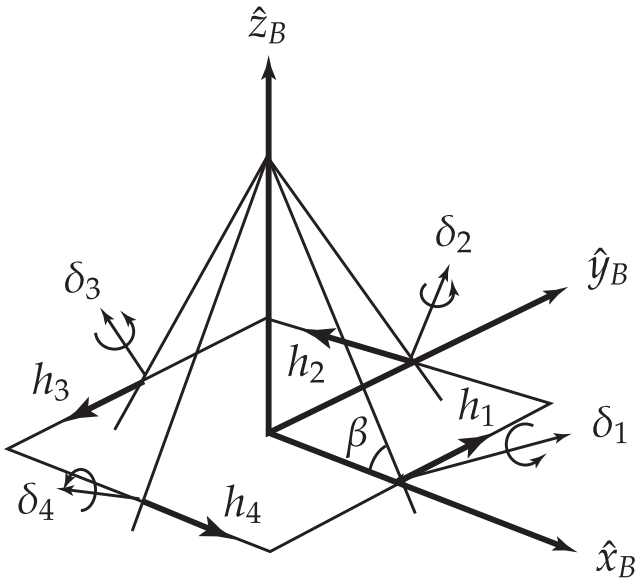

Figure 3.1: Pyramid configuration for four SGCMGs

where $G = G(\delta)$ is the $3 \times N$ Jacobian matrix, N is the number of the CMGs. The gimbal rate command $\dot{\delta} \in \mathbb{R}^N$ is calculated as

$$\dot{\delta} = G^+ T \tag{3.4}$$

where $G^+ = G^T(GG^T)^{-1}$ is the pseudo-inverse of the matrix G.

3.2 Pyramid Array of Four SGCMGs

Setting $N = 4$, here we consider a pyramid array of four SGCMGs as shown in Fig. 3.1, where four SGCMGs are located on the faces of pyramid and the gimbal axes are orthogonal to the pyramid faces. Each SGCMG has the same angular momentum and the skew angle is chosen as $\beta = 54.73$ (deg) so that the momentum envelope becomes nearly spherical. The angular momentum vector h is given as a function of gimbal angle δ as follows:

$$h = h_w \begin{bmatrix} -c\beta \sin\delta_1 - \cos\delta_2 + c\beta \sin\delta_3 + \cos\delta_4 \\ \cos\delta_1 - c\beta \sin\delta_2 - \cos\delta_3 + c\beta \sin\delta_4 \\ s\beta \sin\delta_1 + s\beta \sin\delta_2 + s\beta \sin\delta_3 + s\beta \sin\delta_4 \end{bmatrix} \tag{3.5}$$

where h_w is the magnitude of the angular momentum of a flywheel, $c\beta = \cos\beta$ and $s\beta = \sin\beta$, and the Jacobian matrix G is given by

$$G = h_w \begin{bmatrix} -c\beta\cos\delta_1 & \sin\delta_2 & c\beta\cos\delta_3 & -\sin\delta_4 \\ -\sin\delta_1 & -c\beta\cos\delta_2 & \sin\delta_3 & c\beta\cos\delta_4 \\ s\beta\cos\delta_1 & s\beta\cos\delta_2 & s\beta\cos\delta_3 & s\beta\cos\delta_4 \end{bmatrix} \tag{3.6}$$

3.3 Singularity Analysis of CMG System

A singularity is encountered when there exists some direction for which the array of CMGs is not capable of producing torque. This phenomenon occurs when the gimbal angles of CMGs become some specific arrangement. The $3 \times N$ Jacobian matrix G is a function of the gimbal angles and it has the maximum rank of 3. When rank(G) = 2, all column vectors of Jacobian matrix, g_i ($i = 1, \cdots, N$) become coplanar and there exists a unit vector u^s orthogonal to that coplanar plane; i.e.,

$$G^T u^s = g_i^T u^s = 0, \quad (i = 1, \cdots, N) \tag{3.7}$$

Therefore, the CMG system cannot produce any momentum along the direction of singular vector u^s. As shown in Eq. (3.7), there exists a vector u^s normal to all g_i at the singularity. Therefore, we select u^s as parameter and solve this equation with respect to g_i. Since g_i is perpendicular to both u_s and gimbal axis vector a_i, Eq. (3.7) can be rewritten as

$$g_i^s = \frac{\varepsilon_i (a_i \times u_s)}{|a_i \times u_s|}, \quad (a_i \neq u_s) \tag{3.8}$$

where, $\varepsilon_i = \pm 1$, and subscript s denotes singular point. Let u^s be a unit vector of the punctured unit sphere defined as

$$\mathcal{S} = \{u^s : |u^s| = 1\} \tag{3.9}$$

The angular momentum as a singular point is given by the following equation:

$$h_i^s = g_i^s \times a_i \tag{3.10}$$

At the singular point, all h_i is in the direction that is along with u^s or $-u^s$ as close as possible. By introducing p_i,

$$p_i = \varepsilon_i |a_i \times u^s|^{-1}, \quad (a_i \neq u^s) \tag{3.11}$$

Eq. (3.8) can be rewritten as

$$g_i^s = p_i a_i \times u^s \tag{3.12}$$

Thus, there exists singularities for arbitrary u^s that satisfies Eq. (3.7). If $a_i \neq u^s$, there are 2^N combinations of ε_i for a cluster of N CMG system.

The singularities of the pyramid array of four SGCMGs are derived as follows. The unit vector u^s is parameterized with the azimuth angle $\vartheta_1 \in [0,\ 2\pi]$ and elevation angle $\vartheta_2 \in [0,\ 2\pi]$ in the spherical coordinate as follows:

$$u^s = [u_x^s,\ u_y^s,\ u_z^s]^T = [\sin\vartheta_2,\ -\sin\vartheta_1\cos\vartheta_2,\ \cos\vartheta_1\cos\vartheta_2]^T \tag{3.13}$$

The angular momentum at the singular point, h_i^s is given by Eq. (3.10). Substituting Eq. (3.8) into Eq. (3.10),

$$h_i^s = g_i^s \times a_i = \frac{\varepsilon_i(a_i \times u^s) \times a_i}{|a_i \times u^s|} = \frac{1}{e_i}(a_i \times u^s) \times a_i \tag{3.14}$$

where

$$e_i = \varepsilon_i |a_i \times u^s| = \varepsilon_i \sqrt{1 - (a_i \cdot u^s)^2} \tag{3.15}$$

For a pyramid array, e_i is given as follows:

$$e_1 = \varepsilon_1 \sqrt{1 - (s\beta u_x^s + c\beta u_z^s)^2} \tag{3.16a}$$

$$e_1 = \varepsilon_2 \sqrt{1 - (s\beta u_y^s + c\beta u_z^s)^2} \tag{3.16b}$$

$$e_1 = \varepsilon_3 \sqrt{1 - (-s\beta u_x^s + c\beta u_z^s)^2} \tag{3.16c}$$

$$e_1 = \varepsilon_4 \sqrt{1 - (-s\beta u_y^s + c\beta u_z^s)^2} \tag{3.16d}$$

where $s\beta = \sin\beta$ and $c\beta = \cos\beta$.

The singular surface $(h_x^s,\ h_y^s,\ h_z^s)$, corresponding to the singular vector u^s and singular gimbal angles δ^s, can be obtained as

$$h_x^s = \frac{c\beta(-s\beta u_z^s + c\beta u_x^s)}{e_1} + \frac{u_x^s}{e_2} + \frac{c\beta(s\beta u_z^s + c\beta u_x^s)}{e_3} + \frac{u_x^s}{e_4} \tag{3.17a}$$

$$h_y^s = \frac{u_y^s}{e_1} - \frac{c\beta(s\beta u_z^s - c\beta u_y^s)}{e_2} + \frac{u_y^s}{e_3} + \frac{c\beta(s\beta u_z^s + c\beta u_y^s)}{e_4} \tag{3.17b}$$

$$h_z^s = \frac{s\beta(-c\beta u_x^s + s\beta u_z^s)}{e_1} + \frac{s\beta(s\beta u_z^s - c\beta u_y^s)}{e_2} + \frac{s\beta(s\beta u_z^s + c\beta u_x^s)}{e_3} + \frac{s\beta(s\beta u_z^s + c\beta u_y^s)}{e_4} \tag{3.17c}$$

The singularity surface for the pyramid array is shown in Figs. 3.2 and 3.3. Figure 3.2 shows the singularity surface when all ε_i have the same sign. The sphere singularity surface represents the maximum momentum envelope and they are all sign-definite singularity points. There are eight circular windows on the surface, which corresponds to gimbal axes. Theses circular windows are smoothly connected to the internal singular surface, for which one and only one of the ε_i is negative. This singular surface produces a trumpet-like funnel at the circular windows, which completes the angular momentum envelope and is shown in Fig. 3.3.

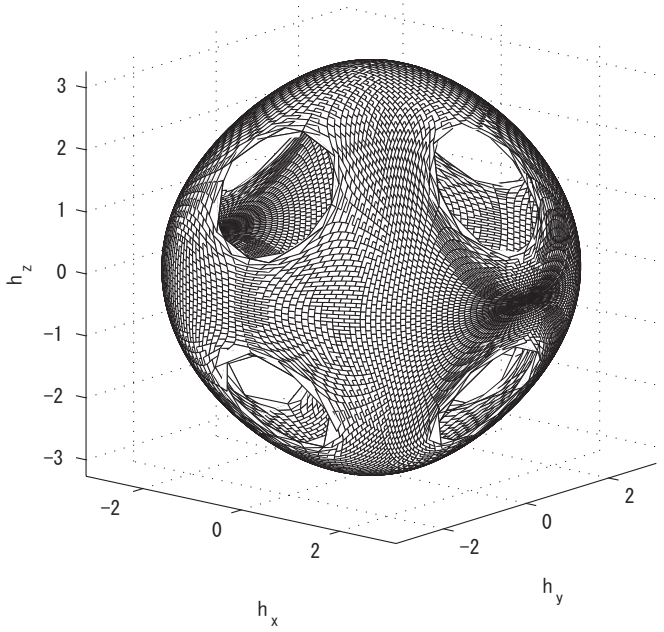

Figure 3.2: Angular momentum envelope ($\varepsilon_1 = \varepsilon_2 = \varepsilon_3 = \varepsilon_4 = +1$)

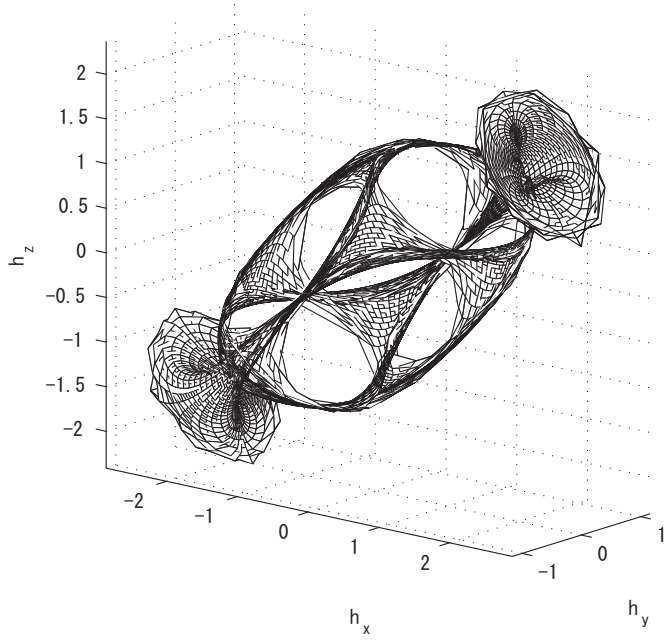

Figure 3.3: Example of an internal singularity ($\varepsilon_1 = -1,\ \varepsilon_2 = \varepsilon_3 = \varepsilon_4 = +1$)

3.4 Singularity Avoidance Using SVD

The sign-definite singular point described in the previous section is *impassable* and this type of singularity cannot be escaped even by use of the SR steering logic. That is, the sign-definite singular point has a characteristic like a wall that cannot be passed through, and one cannot escape from this singularity by using redundancy.

In this section, the author presents a method of singularity avoidance that uses the singular value decomposition to obtain the singular direction and output the torque orthogonal to the singular direction for fast singularity avoidance. This steering method is proposed by Tani et al. [20, 16]. In the following, this method is simply called to " *proposed steering law* " or " *proposed method* ".

First, consider the singular value decomposition of the Jacobian matrix G. For such G, there exist unitary matrices $U \in \mathbb{R}^{3\times3}$ and $V \in \mathbb{R}^{4\times4}$ such that $U^TU = I_3$ and $V^TV = I_4$, and

$$G = U\Sigma V^T \tag{3.18}$$

where

$$\Sigma = \begin{bmatrix} \sigma_1 & 0 & 0 & 0 \\ 0 & \sigma_2 & 0 & 0 \\ 0 & 0 & \sigma_3 & 0 \end{bmatrix} \tag{3.19}$$

The positive numbers, $\sigma_1 \geq \sigma_2 \geq \sigma_3 \geq 0$, are called singular values of matrix G.

From Eq. (3.18), for $1 \leq i \leq 3$, we have

$$(GG^T)U = U(\Sigma\Sigma^T) \quad \text{or} \quad (GG^T)u_i = \sigma_i^2 u_i \tag{3.20a}$$

$$(G^TG)V = V(\Sigma^T\Sigma) \quad \text{or} \quad (G^TG)v_i = \sigma_i^2 v_i \tag{3.20b}$$

where

$$U = [u_1\ u_2\ u_3] \tag{3.21a}$$

$$V = [v_1\ v_2\ v_3\ v_4]^T \tag{3.21b}$$

The column vector u_i and v_i are the left and right singular vectors of matrix G, respectively. The pseudo inverse of matrix G can be expanded with Eq. (3.18) in terms of the singular vectors u_i and v_i as follows:

$$G^+ = V\Sigma^+U^T \tag{3.22}$$

where

$$\Sigma^{+} = \begin{bmatrix} 1/\sigma_1 & 0 & 0 \\ 0 & 1/\sigma_2 & 0 \\ 0 & 0 & 1/\sigma_3 \\ 0 & 0 & 0 \end{bmatrix} \tag{3.23}$$

Therefore, the pseudo inverse steering law in Eq. (3.4) can be written as follows:

$$\dot{\delta} = G^{+}T = \sum_{i=1}^{3} \left(\frac{1}{\sigma_i}\right) v_i u_i^T T \tag{3.24}$$

If σ_i is zero in a singularity, the gimbal rate command diverges to the infinity.

The Singularity Robust (SR) steering law is a method to avoid such a singularity [23]. In this method, the gimbal rate command is given by the following equation:

$$\dot{\delta} = G^{\#}T \tag{3.25}$$

where $G^{\#}$ is called the SR inverse given by

$$G^{\#} = G^T(GG^T + \lambda I)^{-1} \tag{3.26}$$

and λ is a constant positive scalar to be properly selected. Note that

$$G^{\#} = V\Sigma^{\#}U^T \tag{3.27}$$

where

$$\Sigma^{\#} = \begin{bmatrix} \sigma_1/(\sigma_1^2 + \lambda) & 0 & 0 \\ 0 & \sigma_2/(\sigma_2^2 + \lambda) & 0 \\ 0 & 0 & \sigma_3/(\sigma_3^2 + \lambda) \\ 0 & 0 & 0 \end{bmatrix} \tag{3.28}$$

At a singular point with rank(G) = 2 and $\sigma_3 = 0$, vectors u_3 and v_3 represent the singular torque and the singular gimbal rate direction, respectively. Then

$$\dot{\delta} = \sum_{i=1}^{2} \left(\frac{\sigma_i}{\sigma_i^2 + \lambda}\right) v_i u_i^T T \tag{3.29}$$

Now, the author introduces an evaluation function for indicating that the system is approaching to a singularity. The following singularity parameter κ is defined as an index of the degree of singularity:

$$\kappa \triangleq \frac{\sigma_1}{\sigma_3} \tag{3.30}$$

where σ_1 and σ_3 are the maximum and the minimum singular value of matrix G, respectively. The value of κ increases, as the gimbal angles approaches to a singular point with σ_3 being a very small value. The direction of the input torque with maximum gain, u_1, is chosen to generate the torque input that is orthogonal to the critical singular direction u_3. Therefore, the direction of the command gimbal rate is selected as v_1 that corresponds to the torque input direction u_1.

In this chapter, the following steering law is applied.

$$\dot{\delta} = \sum_{i=1}^{3} \left(\frac{\sigma_i}{\sigma_i^2 + \lambda} \right) v_i u_i^T T + k_{SA} SW(\kappa) v_1 \tag{3.31}$$

where $SW(\kappa)$ is a switching function defined as

$$SW(\kappa) = \frac{1}{2} \left(\frac{\kappa - \kappa_d}{| \kappa - \kappa_d |} + 1 \right) \tag{3.32}$$

The first term in Eq. (3.31) is the same as the SR steering law in Eq. (3.25) and the second term is added to escape from the singularities. When κ is smaller than κ_d, the switching function $SW(\kappa) = 0$, and the proposed steering law in Eq. (3.31) reduces to the conventional SR steering law in Eq. (3.25). The right singular vector v_1 is employed in the second term in order to output the maximum torque in the direction orthogonal to the singularity surface, and to escape rapidly from the singular point.

3.5 Fixed-Star Tracking Attitude Control

In this section, the author considers fixed-star tracking attitude control of a spacecraft. Figure 3.4 shows the configuration of fixed-stars. The line-of-sight vector of the remote sensor is aligned along z axis of the body-fixed frame.

A coordinates transformation matrix R_I^B from the inertial frame to the body-fixed frame is defined as

$$\begin{aligned} R_I^B &= \begin{bmatrix} 1 & 0 & 0 \\ 0 & \cos\phi & \sin\phi \\ 0 & -\sin\phi & \cos\phi \end{bmatrix} \begin{bmatrix} \cos\theta & 0 & -\sin\theta \\ 0 & 1 & 0 \\ \sin\theta & 0 & \cos\theta \end{bmatrix} \\ &= \begin{bmatrix} \cos\theta & 0 & -\sin\theta \\ \sin\phi\sin\theta & \cos\phi & \sin\phi\cos\theta \\ \cos\phi\sin\theta & -\sin\phi & \cos\phi\cos\theta \end{bmatrix} \end{aligned} \tag{3.33}$$

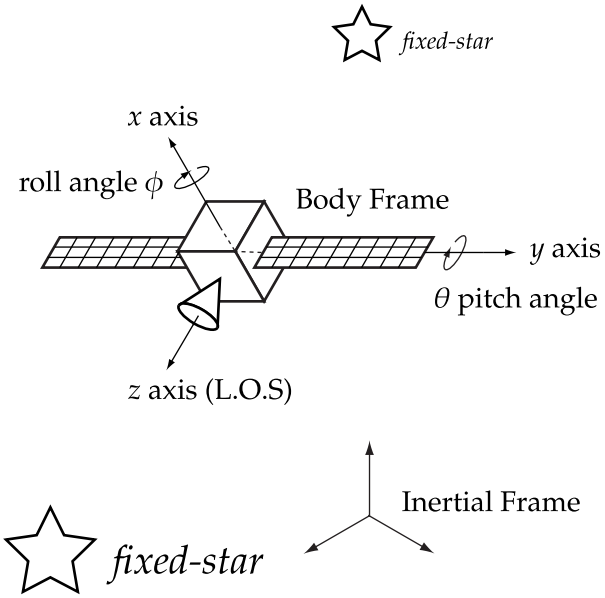

Figure 3.4: Example of the configuration for fixed-stars

where ϕ and θ are the Euler angle about x axis and y axis of the body-fixed frame, respectively. The direction vector of *star i*, for $i = a,\ b$ in the body-fixed frame is defined as $s_i^b = [s_{i1}^b,\ s_{i2}^b,\ s_{i3}^b]^T$. Therefore, the following equation is obtained

$$\begin{bmatrix} s_{i1}^b \\ s_{i2}^b \\ s_{i3}^b \end{bmatrix} = R_I^B \begin{bmatrix} 0 \\ 0 \\ 1 \end{bmatrix} = \begin{bmatrix} -\sin\theta \\ \sin\phi\cos\theta \\ \cos\phi\cos\theta \end{bmatrix} \tag{3.34}$$

From Eq. (3.34), θ and ϕ are calculated as

$$\theta = -\text{asin}\left(s_{i1}^b\right) \tag{3.35a}$$

$$\phi = \text{atan2}\left(\frac{s_{i2}^b}{\cos\theta},\ \frac{s_{i3}^b}{\cos\theta}\right) \tag{3.35b}$$

A PD controller is designed as follows:

$$\tau = -K_p \begin{bmatrix} \phi \\ \theta \\ 0 \end{bmatrix} - K_d \begin{bmatrix} \omega_x \\ \omega_y \\ \omega_z \end{bmatrix} \tag{3.36}$$

where $K_p \in \mathbb{R}^{3\times3}$, $K_d \in \mathbb{R}^{3\times3}$ are the gain matrices.

Table 3.1: Numerical simulation data

Symbol	Value	Units
J	diag[10, 10, 9]	kgm^2
h_w	0.5	Nms
β	54.73	deg
ω_0	$[0, 0, 0]^T$	deg/sec
δ_0	$[0, 0, 0, 0]^T$	deg
$\dot{\delta}_0$	$[0, 0, 0, 0]^T$	rad/sec
$\lvert\dot{\delta}\rvert_{max}$	1	rad/sec
k_{SA}	0.01	–
κ_d	4.0	–
K_p	diag[5, 5, 4.5]	–
K_d	diag[20, 20, 18]	–

3.6 Numerical Simulation

In this section, the author gives the results of the numerical simulations for two cases of the fixed-stars tracking control. The first case is the tracking attitude control for *two fixed-stars*. And the second case is the tracking attitude control for *four fixed-stars*. In order to compare the singularity avoidance performance, we shows the results using both the conventional SR steering law in Eq. (3.25) and the proposed steering law in Eq. (3.31). The spacecraft parameters, the initial condition, and the control gain are given in Table 3.1.

In this paper, the constant positive scalar λ in Ref. [23] is chosen as

$$\lambda = 0.01 \exp\left(-10 \det(GG^T)\right) \tag{3.37}$$

Case 1: Tracking Control for Two Fixed-Stars

The author first gives a numerical example of the tracking control for two fixed stars, *star a* and *star b*. The direction vectors of two fixed stars in the inertial frame are given as

$$s_a = [0,\ 0,\ 1]^T,\ s_b = [0,\ 0,\ -1]^T \tag{3.38}$$

A simulation result of the tracking control with the conventional SR steering law in Eq. (3.25) is shown in Figs. 3.5 and 3.6, and that with the proposed steering law in Eq. (3.31) is shown in Figs. 3.7 and 3.8. In Figs. 3.5 and 3.8, (a) shows the direction angle; (b) the spacecraft angular velocity; (c) the gimbal rate; (d) the gimbal angle; (e) the CMG angular momentum; and (f) the singularity parameter κ. In Figs. 3.5(a) and 3.7(a), the direction angle is given as the angle between z axis (L.O.S) of the body-fixed frame and the line connecting two fixed stars, *star a* and *star b* in the inertial frame.

In Figs. 3.5 and 3.6 associated with the SR steering law in Eq. (3.25), the tracking control of *star a* and *star b* is completed in about 150 sec as shown in Fig. 3.5(a). As seen from Fig. 3.6(d), the CMG system encounters the internal singularity of $\delta = [270,\ 0,\ 90,\ 0]^T$ deg at about 2 sec. The singularity parameter κ becomes large at this time as shown in Fig. 3.6(f). Figure 3.5(b) shows the spacecraft angular velocity. When the CMG system encounters the singularity, the spacecraft angular velocity is uncontrollable. Therefore, the *star a* is tracked in about 75 sec. Similarly, the singularity of $\delta = [90,\ 0,\ 270,\ 0]^T$ deg is encountered at about 77 sec (Fig. 3.6(d)). The *star b* is tracked in about 150 sec (Fig. 3.5(a)).

In Fig. 3.7 and 3.8 associated with the proposed steering law in Eq. (3.31), a singularity is also encountered at about 2 sec, where the CMG system is avoiding the singularity by the output torque in the direction perpendicular to the singular direction. For this reason, the maximum output angular momentum of the CMG system is about 1.56 Nms in the case of the proposed steering law (Fig. 3.8(e)), whereas it is only about 0.56 Nms when the SR steering law is applied (Fig. 3.6(e)).

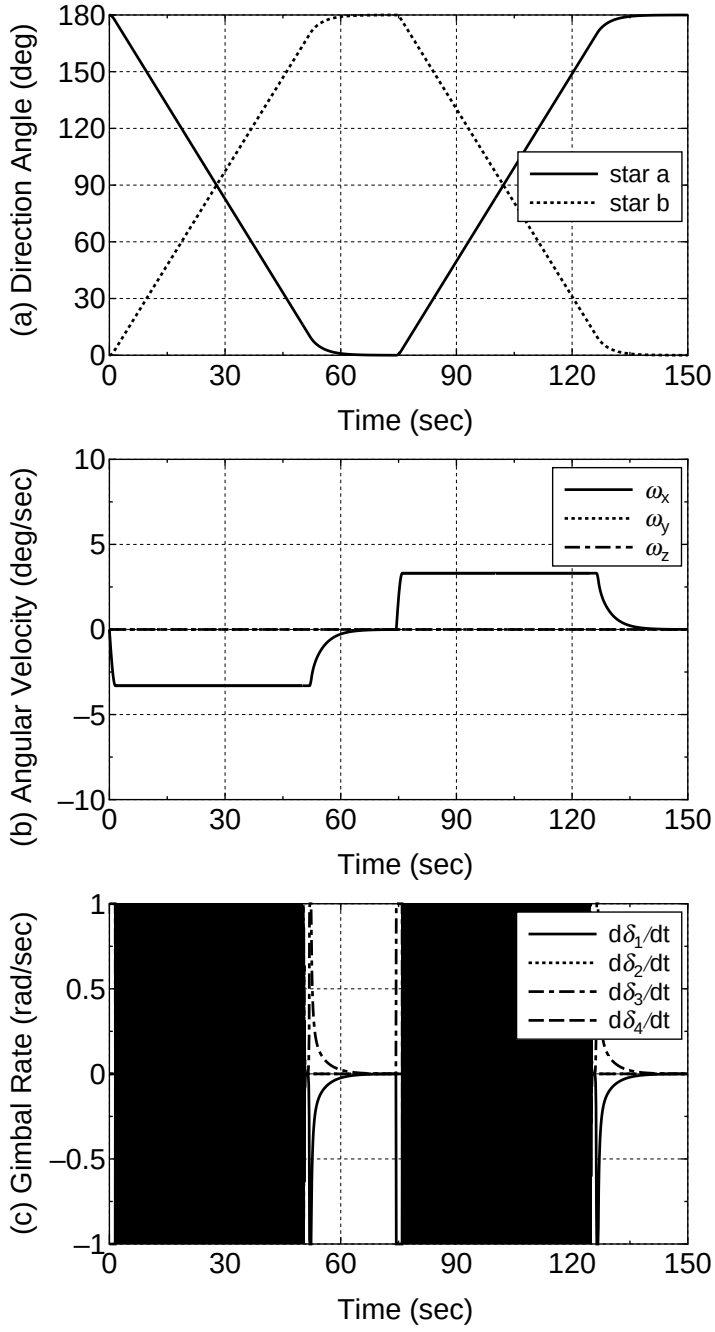

Figure 3.5: Simulation result: **Case 1** (SR steering law)

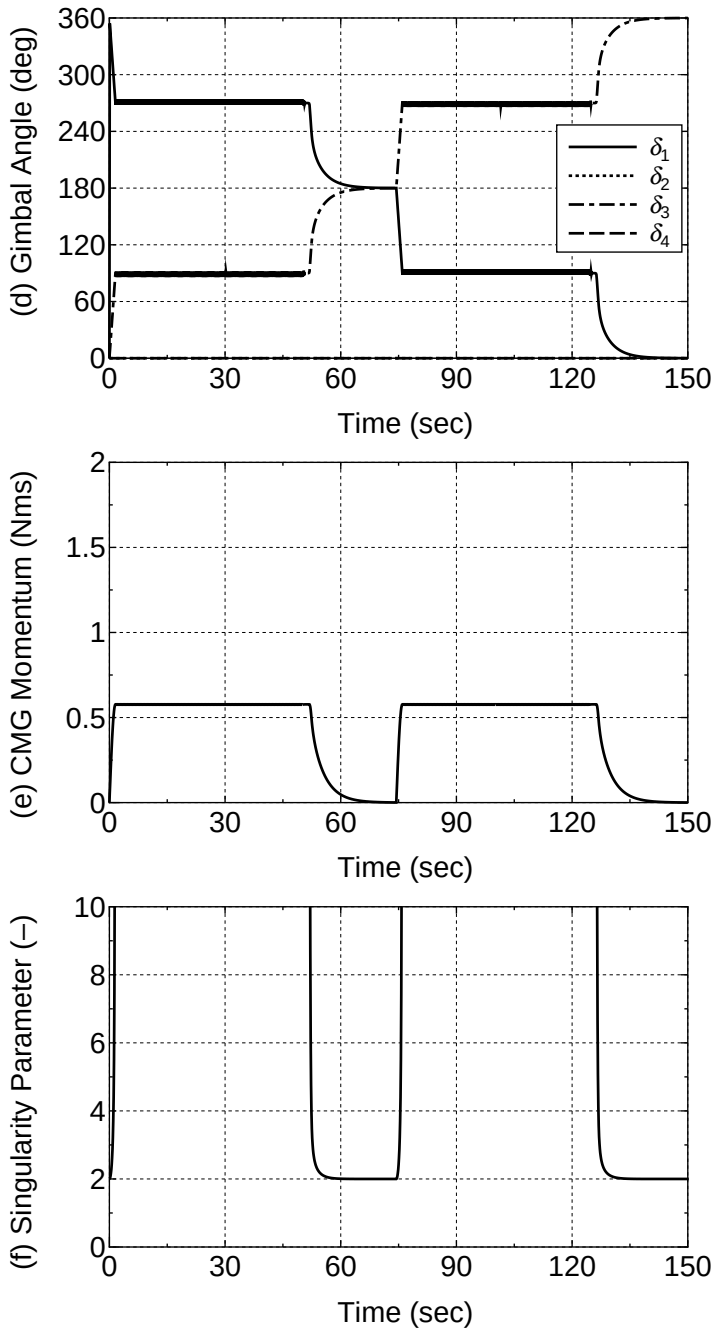

Figure 3.6: Simulation result: **Case 1** (SR steering law)

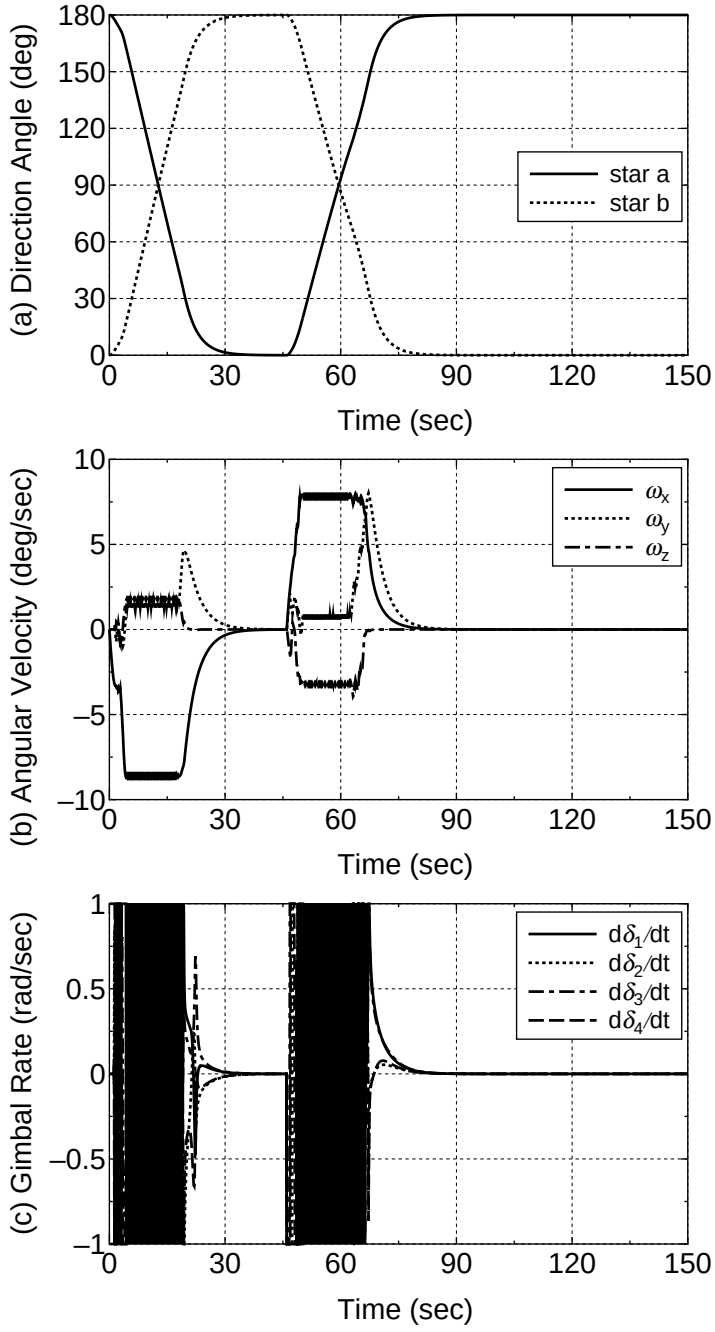

Figure 3.7: Simulation result: **Case 1** (proposed steering law)

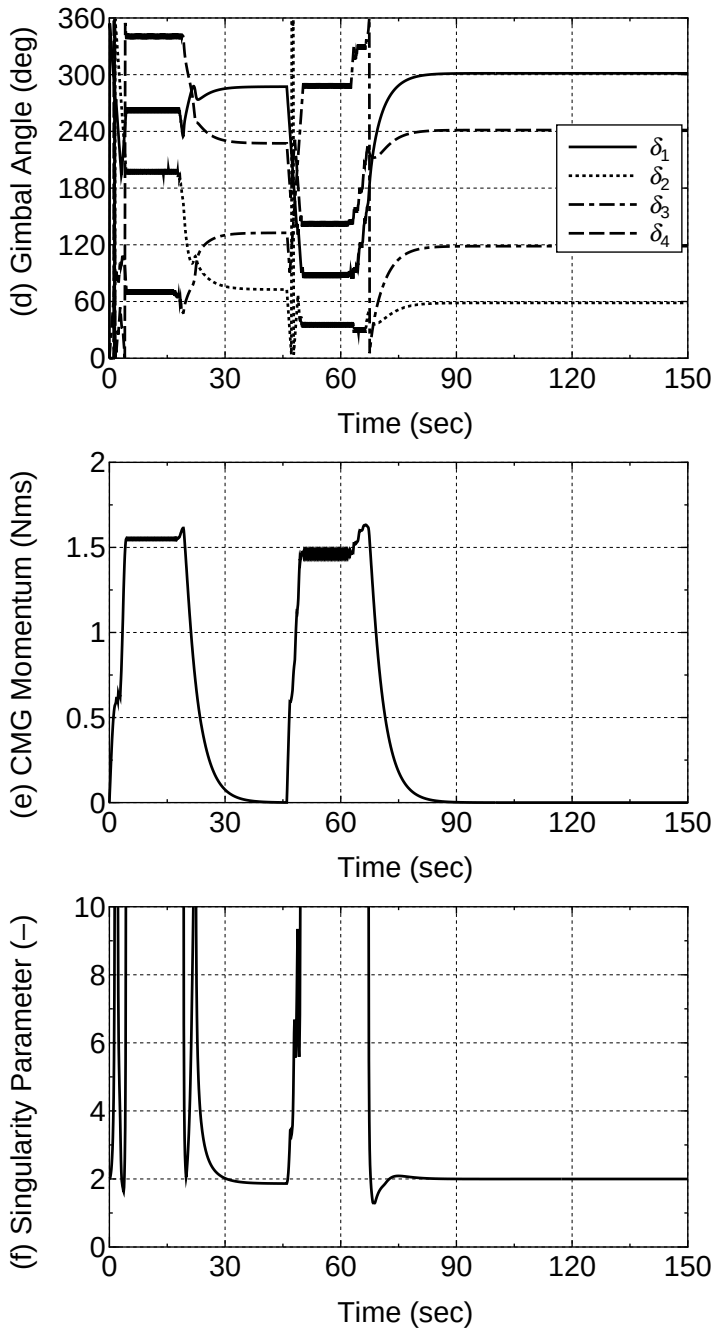

Figure 3.8: Simulation result: **Case 1** (proposed steering law)

Case 2: Tracking Control for Four Fixed-Stars

The author gives a numerical example of the tracking control for four fixed stars, *star a*, *star b*, *star c* and *star d*. Suppose that these fixed-stars exist at the vertex of a regular tetrahedron as shown Fig. 3.9. Then, the direction vectors of four fixed stars in the inertial frame are given as

$$\begin{aligned} s_a &= [0,\ 0,\ 1]^T, \\ s_b &= [\ \sqrt{2}/3,\ 0,\ -1/3]^T, \\ s_c &= [-\sqrt{2}/3,\ \sqrt{6}/3,\ -1/3]^T, \\ s_d &= [-\sqrt{2}/3,\ -\sqrt{6}/3,\ -1/3]^T \end{aligned} \tag{3.39}$$

Moreover, we suppose that the spacecraft locates at the center of the regular tetrahedron. The tracking sequence of fixed-stars from an initial orientation/attitude of the spacecraft is as follows:

$$star\ a \rightarrow star\ b \rightarrow star\ c \rightarrow star\ d$$

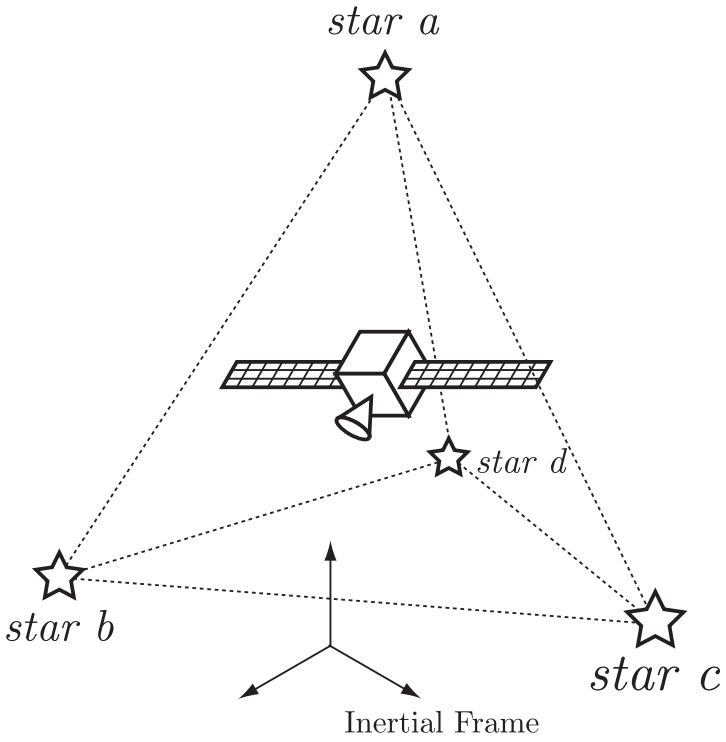

Figure 3.9: Configuration of four fixed-stars

A simulation result of the tracking control with the conventional SR steering law in Eq. (3.25) is shown in Figs. 3.10 and 3.11, and that with the proposed steering law in Eq. (3.31) is shown in Figs. 3.12 and 3.13. In Figs. 3.10 and 3.13, (a) shows the direction angle; (b) the spacecraft angular velocity; (c) the gimbal rate; (d) the gimbal angle; (e) the CMG angular momentum; and (f) the singularity parameter κ. In Figs. 3.10(a) and 3.12(a), the direction angle is given as the angle between z axis (L.O.S) of the body-fixed frame and the line connecting four fixed stars, *star a*, *star b*, *star c* and *star d* in the inertial frame.

In Fig. 3.10(a), the *star a* tracking control with the SR steering law is 75 sec. As seen from Fig. 3.11(d), the CMG system encounters the singularity at about 2 sec. Moreover, the singularity parameter κ becomes large at about 2 sec as shown in Fig. 3.11(f). In Fig. 3.11(a), the *star a* tracking control with the proposed steering law is 45 sec.

However, it cannot be shown that the significant difference of both steering laws in the singularity avoidance capability for tracking *star b*, *star c* and *star d*. For this fact, it can be thought that external singularities (i.e., the angular momentum envelope) are encountered while tracking each stars. As shown in Figs. 3.11(e) and 3.13(e), the CMG angular momentum become maximum value at the external singularity.

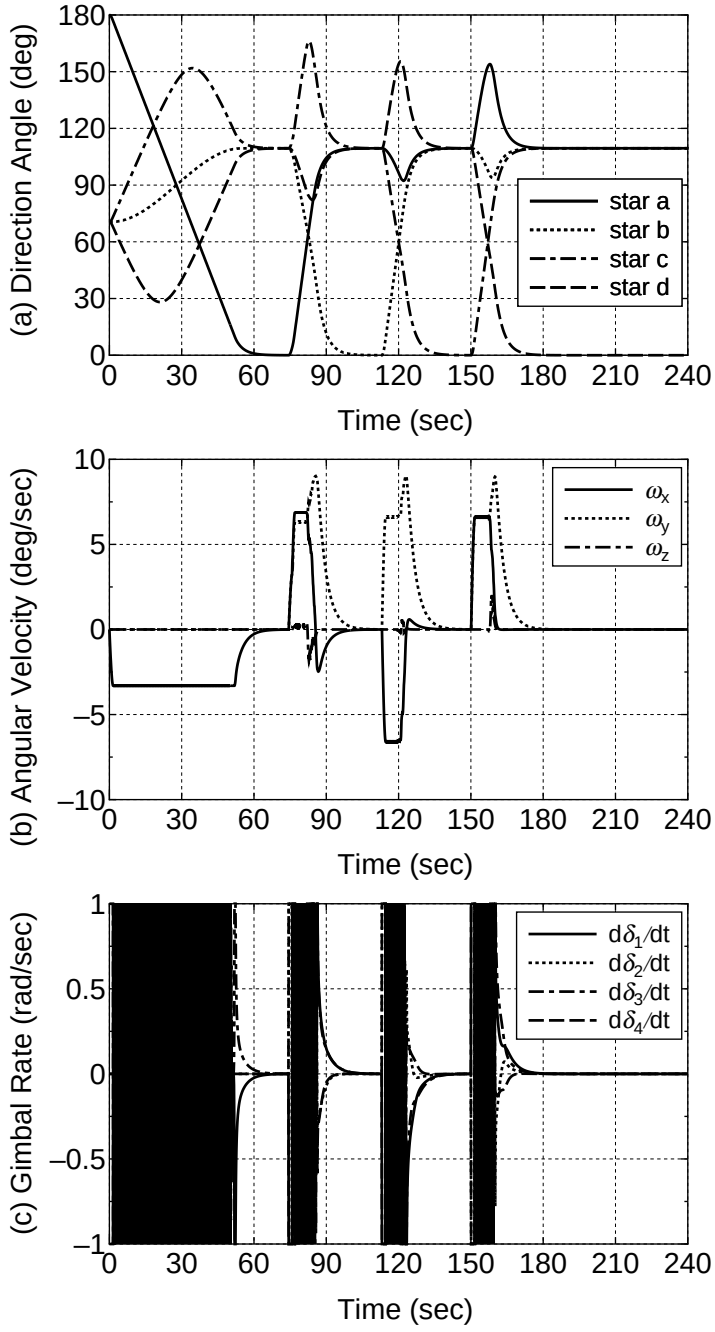

Figure 3.10: Simulation result: **Case 2** (SR steering law)

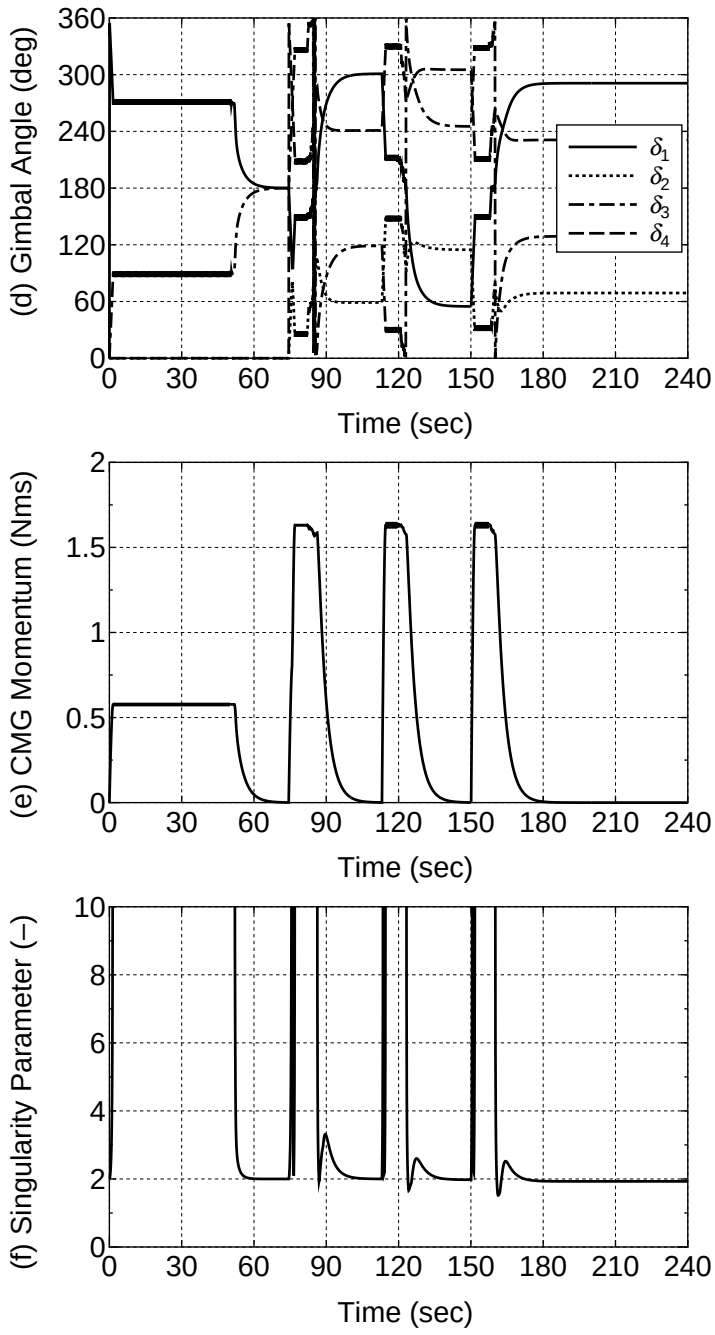

Figure 3.11: Simulation result: **Case 2** (SR steering law)

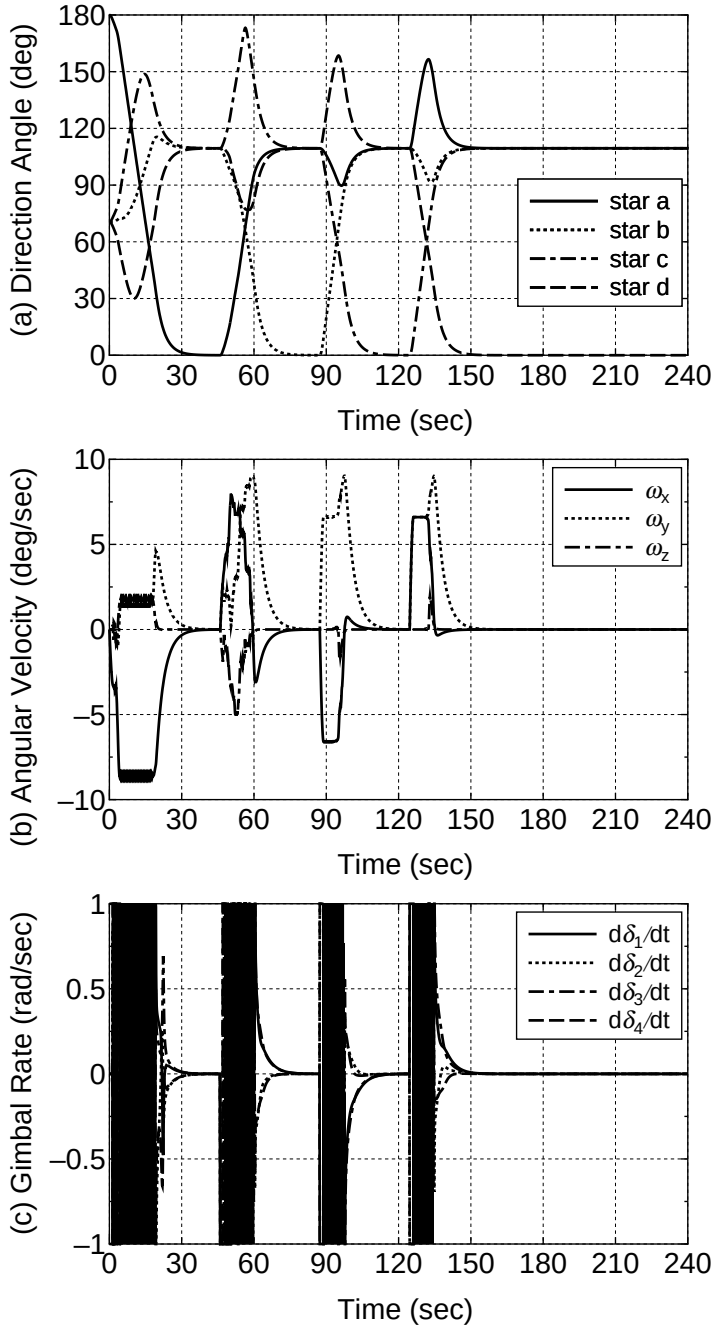

Figure 3.12: Simulation result: **Case 2** (proposed steering law)

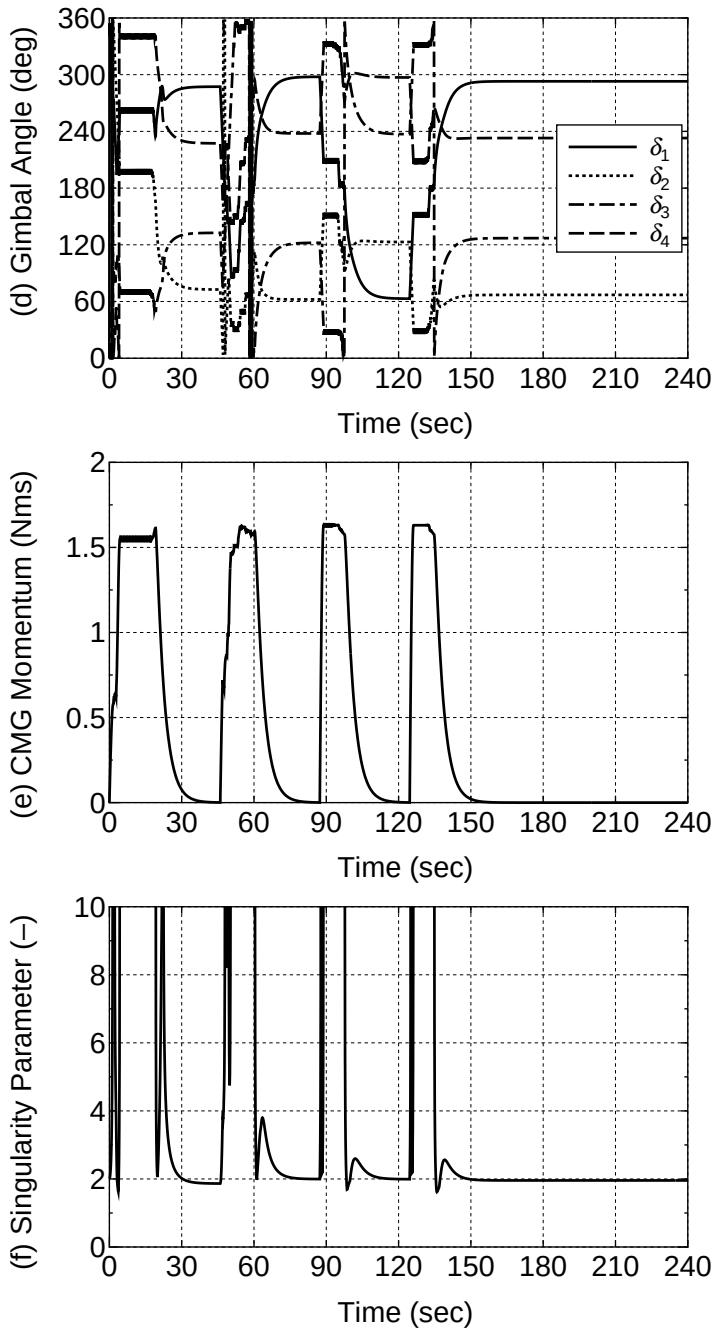

Figure 3.13: Simulation result: **Case 2** (proposed steering law)

3.7 Conclusion

In this chapter, a cluster of 4-SGCMGs in pyramid type configuration has been studied for fixed-stars tracking attitude control of small satellites. The singularities of the steering logic have been investigated to show the singularity surfaces in three-dimensional angular momentum space.

The proposed method utilizes the singular value decomposition to obtain the singular vector and generates the command gimbal rate that keeps the command torque in the direction orthogonal to the singular direction with maximum gain.

The result of the numerical simulation demonstrates the advantage of the proposed method in singularity avoidance over the conventional SR steering law. The SR algorithm simply utilizes an artificially perturbed command torque in order to avoid the singularity, whereas the present method efficiently generates the command torque in the direction orthogonal to the singular direction with a maximum gain to escape from the singular point rapidly.

Chapter 4

Pointing Attitude Control of Spacecraft Using Two SGCMGs

4.1 Spacecraft Model with Twin CMG System

In this chapter, we deal with a spacecraft model as shown in Fig. 4.1. The spacecraft model is a rigid body and has the twin CMG system, in which gimbal axes of two SGCMGs are parallel to $\hat{z}_B$ of the body frame $\mathcal{F}_B$. Therefore, the CMG angular momentum vector is produced only in the $(\hat{x}_B - \hat{y}_B)$ plane. We assume that a camera or an antenna is fixed on the body, and their line-of-sight is corresponding to the $\hat{x}_B$ of the body frame. For the twin CMG system of two SGCMGs, the CMG angular momentum vector h is a function of the gimbal angle vector $\delta = [\delta_1,\ \delta_2]^T$ as follows:

$$h(\delta) = h_w \begin{bmatrix} \cos\delta_1 + \cos\delta_2 \\ \sin\delta_1 + \sin\delta_2 \\ 0 \end{bmatrix} \tag{4.1}$$

where h_w is the magnitude of the angular momentum of the flywheel as a constant value. From this equation, we can recall that the CMG angular momentum vector h must be in the $(\hat{x}_B - \hat{y}_B)$ plane.

For ease of analysis, we define a new gimbal angle vector $\gamma = [\gamma_1,\ \gamma_2]^T$ as follows:

$$\gamma_1 \triangleq \frac{\delta_1 + \delta_2}{2} \tag{4.2a}$$

$$\gamma_2 \triangleq \frac{\delta_2 - \delta_1}{2} \tag{4.2b}$$

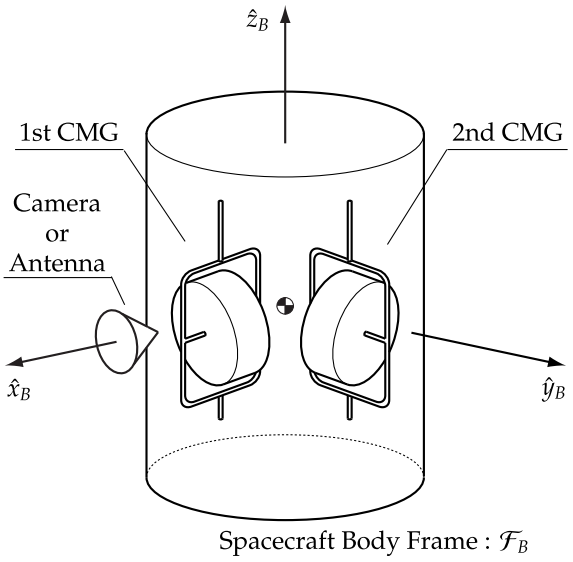

Figure 4.1: The rigid spacecraft model with two SGCMGs

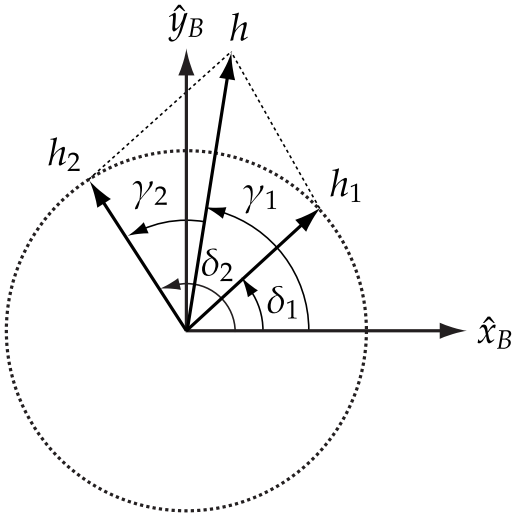

Figure 4.2: Geometrical configuration with a new gimbal angle γ

where γ_1 and γ_2 are called the rotation angle and the scissor angle, respectively [3]. It should be noted that the direction and the magnitude of the CMG angular momentum vector h are respectively determined by the rotation angle γ_1 and the scissor angle γ_2 as shown in Fig. 4.2. By using the new gimbal angle vector γ, the CMG angular momentum vector $h(\delta)$ in Eq. (4.1) can be rewritten as

$$h(\gamma) = 2h_w \begin{bmatrix} \cos\gamma_1 \cos\gamma_2 \\ \sin\gamma_1 \cos\gamma_2 \\ 0 \end{bmatrix} \tag{4.3}$$

The Jacobian matrix $G(\gamma) \in \mathbb{R}^{3\times 2}$ is defined by

$$G(\gamma) = 2h_w \begin{bmatrix} -\sin\gamma_1 \cos\gamma_2 & -\cos\gamma_1 \sin\gamma_2 \\ \cos\gamma_1 \cos\gamma_2 & -\sin\gamma_1 \sin\gamma_2 \\ 0 & 0 \end{bmatrix} \tag{4.4}$$

Thus, the dynamical equation of motion of a rigid spacecraft with two SGCMGs is obtained as

$$J\dot{\omega} = -\omega^{\times}(J\omega + h(\gamma)) - G(\gamma)\dot{\gamma} \tag{4.5}$$

where $\dot{\gamma} = [\dot{\gamma}_1,\ \dot{\gamma}_2]^T$ is the control input.

For a $z-x-z$ Euler angle, the kinematic differential equation is given by

$$\begin{bmatrix} \dot{\phi} \\ \dot{\theta} \\ \dot{\psi} \end{bmatrix} = \begin{bmatrix} \sin\psi \operatorname{cosec}\theta & \cos\psi \operatorname{cosec}\theta & 0 \\ \cos\psi & -\sin\psi & 0 \\ -\sin\psi \cot\theta & -\cos\psi \cot\theta & 1 \end{bmatrix} \begin{bmatrix} \omega_x \\ \omega_y \\ \omega_z \end{bmatrix} \tag{4.6}$$

where $\phi, \psi \in (-180^\circ,\ 180^\circ]$ and $\theta \in (0^\circ,\ 180^\circ)$.

4.2 Pointing Attitude Control Problem

Our pointing attitude control problem is to make the line-of-sight of a camera or an antenna that is fixed on a body axis aim along a desired direction.

4.2.1 Final Attitude of Spacecraft

Due to the angular momentum conservation principle, the total angular momentum of the spacecraft, H is conserved in the inertial frame during a maneuver. It implies that if

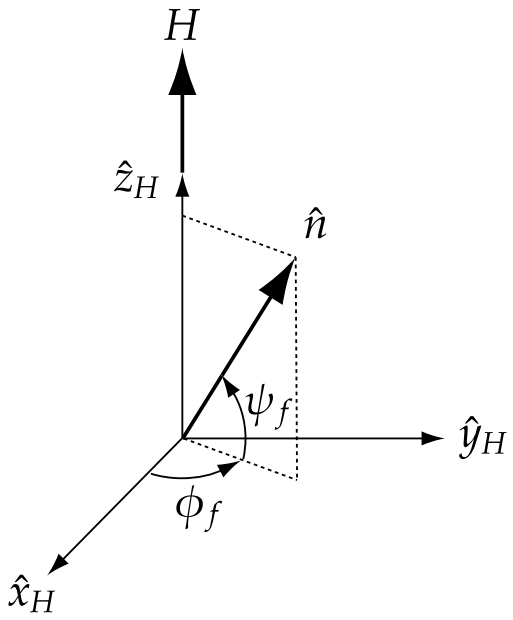

Figure 4.3: Desired direction vector $\hat{n}$ in the inertial frame $\mathcal{F}_H$. Note that this shows a general case with $\theta = 90°$. Actually, $\phi_f = 0°$ or $180°$ in this study.

the angular velocity of the spacecraft is zero, the total CMG angular momentum vector h is aligned with the total angular momentum vector of the spacecraft H. Namely,

$$H = 2h_w \begin{bmatrix} \cos\gamma_{1f}\cos\gamma_{2f} \\ \sin\gamma_{1f}\cos\gamma_{2f} \\ 0 \end{bmatrix} = H_0 \begin{bmatrix} \cos\gamma_{1f} \\ \sin\gamma_{1f} \\ 0 \end{bmatrix} \tag{4.7}$$

where the subscript f denotes the final state, H_0 is the magnitude of the total momentum vector of the spacecraft, H, given as $H_0 \triangleq \|H\| = 2h_w \cos\gamma_{2f}$.

To solve our pointing control problem, we define an inertial frame $\mathcal{F}_H$ which is represented by the orthonormal set of unit vectors $\hat{x}_H$, $\hat{y}_H$ and $\hat{z}_H$ as shown in Fig. 4.3. The unit vector $\hat{z}_H$ is defined as follows:

$$\hat{z}_H \triangleq \frac{H}{H_0} \tag{4.8}$$

Given a desired direction vector $\hat{n}$, which is expressed in the inertial frame $\mathcal{F}_H$, the remaining unit vectors $\hat{y}_H$, $\hat{x}_H$ are given by

$$\hat{y}_H \triangleq \frac{\hat{z}_H \times \hat{n}}{\|\hat{z}_H \times \hat{n}\|}, \quad \hat{x}_H \triangleq \hat{y}_H \times \hat{z}_H \tag{4.9}$$

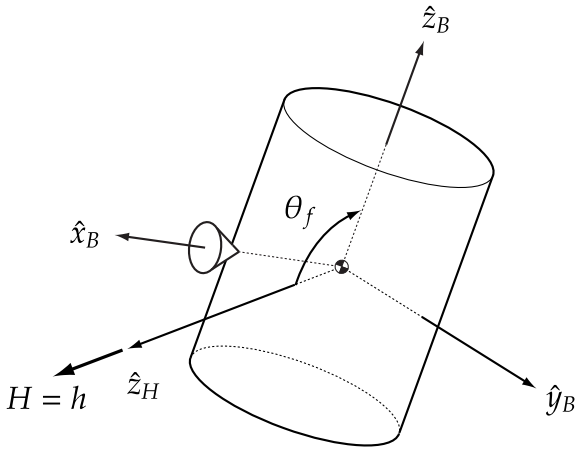

Figure 4.4: The Euler angle θ_f when the spacecraft is at rest, is given by the angle between $\hat{z}_H$ and $\hat{z}_B$. Since $\hat{z}_H$ lies in the $(\hat{x}_b, \hat{y}_B)$ plane, θ_f must be 90°.

A spacecraft orientation can be described by the $z-x-z$ Euler angle from the inertial frame $\mathcal{F}_H$ to the body frame $\mathcal{F}_B$. Then the coordinates transformation matrix is defined by $R_H^B = R_z(\psi)R_x(\theta)R_z(\phi)$, that is

$$R_H^B = \begin{bmatrix} c\phi c\psi - s\phi c\theta s\psi & s\phi c\psi + c\phi c\theta s\psi & s\theta s\psi \\ -c\phi s\psi - s\phi c\theta c\psi & -s\phi s\psi + c\phi c\theta c\psi & s\theta c\psi \\ s\phi s\theta & -c\phi s\theta & c\theta \end{bmatrix} \tag{4.10}$$

where $cj = \cos j$, $sj = \sin j$, for $j = \phi,\ \theta,\ \psi$. From Eqs. (4.7), (4.8) and (4.9), we obtain

$$\begin{bmatrix} \cos\gamma_{1f} \\ \sin\gamma_{1f} \\ 0 \end{bmatrix} = R_H^B \begin{bmatrix} 0 \\ 0 \\ 1 \end{bmatrix} = \begin{bmatrix} \sin\theta_f \sin\psi_f \\ \sin\theta_f \cos\psi_f \\ \cos\theta_f \end{bmatrix} \tag{4.11}$$

It should be noted that the Euler angle θ_f is always 90°, because $\cos\theta_f = 0$ in the third row of Eq. (4.11). It implies that if the spacecraft angular velocity is converged to zero, the Euler angle θ is always converged to $\theta_f = 90°$ since the CMG angular momentum is perpendicular to $\hat{z}_B$ as shown in Fig. 4.4. (Recall that the CMG angular momentum vector h must be in the $(\hat{x}_B - \hat{y}_B)$ plane.

By substituting $\theta_f = 90°$ into the first or second rows of Eq.(4.11), the relation between the final rotation angle γ_{1f} and the final Euler angle ψ_f is obtained as

$$\gamma_{1f} = 90° - \psi_f \tag{4.12}$$

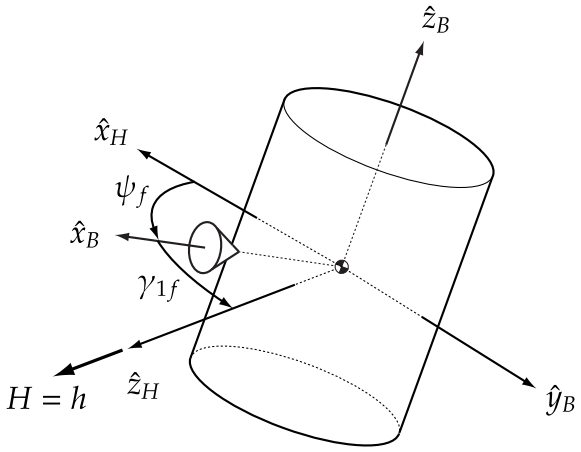

Figure 4.5: The Euler angle ψ_f when the spacecraft is at rest, is given by the angle between $\hat{x}_H$ and $\hat{x}_B$. The direction of the CMG angular momentum vector h is determined by the rotation angle γ_{1f} as the angle between $\hat{x}_B$ and $\hat{z}_H$. Since $\hat{x}_H$ is perpendicular to $\hat{z}_H$, γ_{1f} is given by $\gamma_{1f} = 90^\circ - \psi_f$.

Ii implies that if the spacecraft angular velocity is converged to zero, the above relation (4.12) holds since $\hat{x}_H$ is perpendicular to $\hat{z}_H$ as shown in Fig. 4.5. (Recall that the direction of the CMG angular momentum vector h is determined by the rotation angle γ_1.) Moreover, a final scissor angle γ_{2f} is determined from $H_0 \triangleq 2h_w \cos\gamma_{2f}$ as follows:

$$\gamma_{2f} = \cos^{-1}\left(\frac{H_0}{2h_w}\right) \tag{4.13}$$

Because the domain of function " *arccos* " is given by $[-1, 1]$, we define the range of $H_0/2h_w \in [-1, 1]$ in this study.

Next, a desired direction vector $\hat{n}$ can be expressed in the inertial frame $\mathcal{F}_H$ as $\hat{n} = n_x\hat{x}_H + n_y\hat{y}_H + n_z\hat{z}_H$. We examine the unit vector $\hat{x}_B$ of the body frame $\mathcal{F}_B$ is aligned to a desired direction vector $\hat{n}$, which is obtained as

$$\begin{bmatrix} n_x \\ n_y \\ n_z \end{bmatrix} = R_B^H \begin{bmatrix} 1 \\ 0 \\ 0 \end{bmatrix} = \begin{bmatrix} \cos\phi_f \cos\psi_f \\ \sin\phi_f \cos\psi_f \\ \sin\psi_f \end{bmatrix} \tag{4.14}$$

The right-hand side of Eq. (4.14) is the expression of the desired direction vector $\hat{n}$ in the spherical coordinate system, as shown in Fig. 4.3. Therefore, the desired direction vector $\hat{n}$ can be expressed by the final Euler angles ϕ_f, ψ_f in the inertial frame $\mathcal{F}_H$.

Because the desired direction vector $\hat{n}$ is orthogonal to the vector $\hat{y}_H$ from Eq. (4.9), $n_y = \sin\phi_f \cos\psi_f = 0$. This implies that $\sin\phi_f = 0$ or $\cos\psi_f = 0$. In the case of $\cos\psi_f = 0$, the desired direction vector $\hat{n}$ is parallel to the total angular momentum vector of the spacecraft H from Eq. (4.14). Such special cases are not considered in the study. When, $\sin\phi_f = 0$, it implies that $\phi_f = 0°$ or $\phi_f = 180°$. From Eq. (4.14), $\hat{n} = [\pm\cos\psi_f,\ 0,\ \sin\psi_f]^T$. Therefore, the final Euler angle ψ_f is calculated as

$$\psi_f = \text{atan2}(n_z, \pm n_x) \tag{4.15}$$

This study considers only the case of $\phi_f = 0$.

Therefore, the control objective for pointing control of the spacecraft using two SGCMGs are as follows:

$$\omega \to 0 \tag{4.16a}$$

$$\gamma_{1e} \triangleq \gamma_1 - \gamma_{1f} \to 0 \tag{4.16b}$$

$$\phi_e \triangleq \phi - \phi_f \to 0 \tag{4.16c}$$

where γ_{1e} is the rotation angle error, and ϕ_e is the error of the Euler angle ϕ. In next section, we design a controller for the above control objective.

4.3 Linear Controller Design

In this section, we design a controller for the control objective. First, we linearize the nonlinear system about the equilibrium points, and then investigate the controllability for the linearized system. Next, we design an LQR controller as a simpler method for the linearized system.

4.3.1 Linearization of Nonlinear Spacecraft System

The nonlinear system in Eq. (4.5) can be linearized for the equilibrium points $\omega = 0$, $\gamma_e = 0$ as follows:

$$\dot{\omega} = J^{-1} h_f^{\times} \omega - J^{-1} G_f \dot{\gamma} \tag{4.17}$$

where $h_f^{\times}$ is the skew-symmetric matrix in Eq. (4.17) for h with a final gimbal angle γ_f, and G_f is a matrix which is obtained by substituting the final gimbal angle γ_f into the Jacobian matrix G. The differential equation for the rotation angle error γ_{1e} is given by

$$\dot{\gamma}_{1e} = \dot{\gamma}_1 = u_1 \tag{4.18}$$

The differential equation for the Euler angle error ϕ_e in Eq. (4.6) can be linearized as

$$\dot{\phi}_e = \dot{\phi} = [\sin\psi \operatorname{cosec}\theta,\ \cos\psi \operatorname{cosec}\theta,\ 0]\omega \approx \frac{h_f^T}{h_0}\omega \tag{4.19}$$

This is because $\operatorname{cosec}\theta \approx 1$. Moreover, using the relation of Eq. (4.12), $\sin\psi_f \approx \cos\gamma_{1f}$, $\cos\psi_f \approx \sin\gamma_{1f}$ about the equilibrium point. From Eqs. (4.17) - (4.19), we can obtain the state equation with state vector $x = [\omega^T,\ \gamma_{1e},\ \phi_e]^T \in \mathbb{R}^5$ as follows:

$$\dot{x} = Ax + Bu \tag{4.20}$$

where:

$$A = \begin{bmatrix} J^{-1}h_f^{\times} & 0 & 0 \\ 0 & 0 & 0 \\ h_0^{-1}h_f^T & 0 & 0 \end{bmatrix},\ B = \begin{bmatrix} -J^{-1}g_{1f} & -J^{-1}g_{2f} \\ 1 & 0 \\ 0 & 0 \end{bmatrix}$$

where g_{if}, for $i = 1,\ 2$ is the ith column vector of the matrix G_f, and $u = \dot{\gamma}$ is the control input.

4.3.2 Controllability of Linear System

A necessary and sufficient condition for the controllability of the linearized system in Eq. (4.20) is that the controllability matrix defined as

$$\mathcal{M}_c = [B,\ AB,\ A^2B,\ A^3B,\ A^4B]^T \tag{4.21}$$

has rank five for $\gamma_{1f} \in (-180^\circ,\ 180^\circ]$ and $\gamma_{2f} \in [0^\circ,\ 180^\circ]$. If the final scissor angle γ_{2f} is 0° or 180°, the controllability matrix $\mathcal{M}_c$ for the linearized system in Eq. (4.20) has rank three, and the linearized system is uncontrollable.

4.3.3 LQR Controller

The linear controller to achieve the control objective discussed in section 4.2 is designed on the basis of the LQR theory. Consider the state feedback controller:

$$u = \dot{\gamma} = -Kx \tag{4.22}$$

where $x = [\omega^T,\ \gamma_{1e},\ \phi_e]^T \in \mathbb{R}^5$ is the state vector, and $K \in \mathbb{R}^{2\times5}$ is the control gain matrix, which minimizes the performance index as follows:

$$\mathcal{J} = \int_0^\infty (x^TQx + u^TRu)dt \tag{4.23}$$

where $Q = Q^T \in \mathbb{R}^{5\times5}$ is a positive semidefinite matrix, and $R = R^T \in \mathbb{R}^{2\times2}$ is a positive definite matrix. The control gain matrix K is given by $K = R^{-1}B^TP$. A positive semidefinite matrix $P = P^T$ satisfies the algebraic Riccati equation as follows:

$$A^TP + PA - PBR^{-1}B^TP + Q = 0 \tag{4.24}$$

4.4 Nonlinear Controller Design

In the previous section, we had discussed the design of the LQR controller for a linearized system. However, the LQR controller guarantees local asymptotic stability only around the equilibrium points. In this section, we propose a nonlinear controller that is developed on the basis of Lyapunov stability theory for the stabilization of the gimbal angle error and the angular velocity.

4.4.1 Stabilization of Gimbal Angle Error and Angular Velocity

We consider a continuously differentiable Lyapunov function candidate as follows:

$$\mathcal{V} = \frac{1}{2}\omega^TJ\omega + \frac{1}{2}k\gamma_e^T\gamma_e \tag{4.25}$$

where $k > 0$ is a positive constant. The time derivative of the Lyapunov function, $\dot{\mathcal{V}}$ can be written as

$$\begin{aligned}\dot{\mathcal{V}} &= \omega^TJ\dot{\omega} + k\gamma_e^T\dot{\gamma}_e \\ &= \omega^T\left(-\omega^\times(J\omega + h) - G\dot{\gamma}\right) + k\gamma_e^T\dot{\gamma}_e \\ &= -\omega^TG\dot{\gamma} + k\gamma_e^T\dot{\gamma} \\ &= -(\omega^TG - k\gamma_e^T)\dot{\gamma}\end{aligned} \tag{4.26}$$

The following control input is proposed:

$$\dot{\gamma} = K_n(\omega^TG - k\gamma_e^T)^T \tag{4.27}$$

where $K_n \in \mathbb{R}^{2\times2} > 0$ is a positive-definite gain matrix. Therefore, stabilization of the gimbal angle error and the angular velocity is provided by the proposed control input.

By substituting the proposed control input obtained from Eq. (4.27) into Eq. (4.26), we obtain

$$\dot{\mathcal{V}} = -(\omega^TG - k\gamma_e^T)K_n(\omega^TG - k\gamma_e^T)^T \leq 0 \tag{4.28}$$

However, when $G^T\omega = 0$ and $\gamma_e = 0$, the time derivative of the Lyapunov function, $\dot{\mathcal{V}}$ is zero at the non-trivial equilibrium points.

Table 4.1: Numerical simulation data

Symbol	Value	Units
J	diag[10, 10, 9]	kgm^2
h_w	0.5	Nms
ω_0	$[0.06,\ 0.05,\ -0.05]^T$	rad/s
γ_0	$[90,\ 90]^T$	deg
$\dot{\gamma}_0$	$[0,\ 0]^T$	deg/s
Q	diag[10^5, 10^5, 10^5, 10^0, 10^2]	–
R	diag[10^5, 10^5]	–
K_n	diag[1.7, 1.7]	–
k	0.01	–

4.5 Numerical Simulation

In this section, we present the results of the numerical simulations of the pointing control problem. The parameters of a spacecraft model with two SGCMGs, the initial condition, and the control gain are given in Table 4.1.

For the initial condition in Table 4.1, the LQR controller cannot stabilize the system. Therefore, two steps of the control method are shown as follows:

Mission start

$\downarrow$

1st step: nonlinear controller in Eq. (4.27) for $\omega, \gamma_{1e} \to 0$

$\downarrow$

2nd step: LQR controller in Eq. (4.22) for $\omega, \gamma_{1e}, \phi_e \to 0$

$\downarrow$

Mission complete

The results of the numerical simulations are shown for two cases of pointing control with different target pointing directions.

Case 1: Pointing Control to $\hat{n} = [0.6081, 0, 0.7938]^T$
The unit vector $\hat{x}_B$ of the $\mathcal{F}_B$ is aligned with the desired direction vector $\hat{n} = [0.6081, 0, 0.7938]^T$ in the $\mathcal{F}_H$.

The results of the numerical simulations are shown in Figs. 4.6 and 4.7. These figures show (a) the Euler angle, (b) the spacecraft angular velocity, (c) the gimbal rate, (d) the gimbal angle, (e) the CMG angular moment, and (f) the singularity parameter (i.e., $\det(G^T G)$).

As shown in Fig. 4.6(b), the angular velocity ω, obtained using the nonlinear controller of Eq. (4.27), converges to almost zero at about 190 sec. Moreover, as shown in Fig. 4.6(a), the Euler angles θ and ψ converge to the final values as $\theta_f = 90^\circ$ and $\psi_f = 52.54^\circ$, respectively.

Figure 4.7(d) shows that the rotation angle $\gamma_1$approaches to the final angle $\gamma_{1f} = 37.46^\circ$ in accordance with Eq. (4.12). In Fig. 4.6(c), we can show that both the rotation angle γ_1 and the scissor angle γ_2 are used as control input during the 1st step.

At 190 sec, the nonlinear controller is switched to the LQR controller of the 2nd step using Eq. (4.22). During the 2nd step, only the scissor angle is used to make $\phi \to 0$ as shown in Fig. 4.7(d). Figure 4.6(a) shows that the Euler angle ϕ smoothly converges to $\phi_f = 0^\circ$ and that the pointing control of the satellite is completed at about 320 sec.

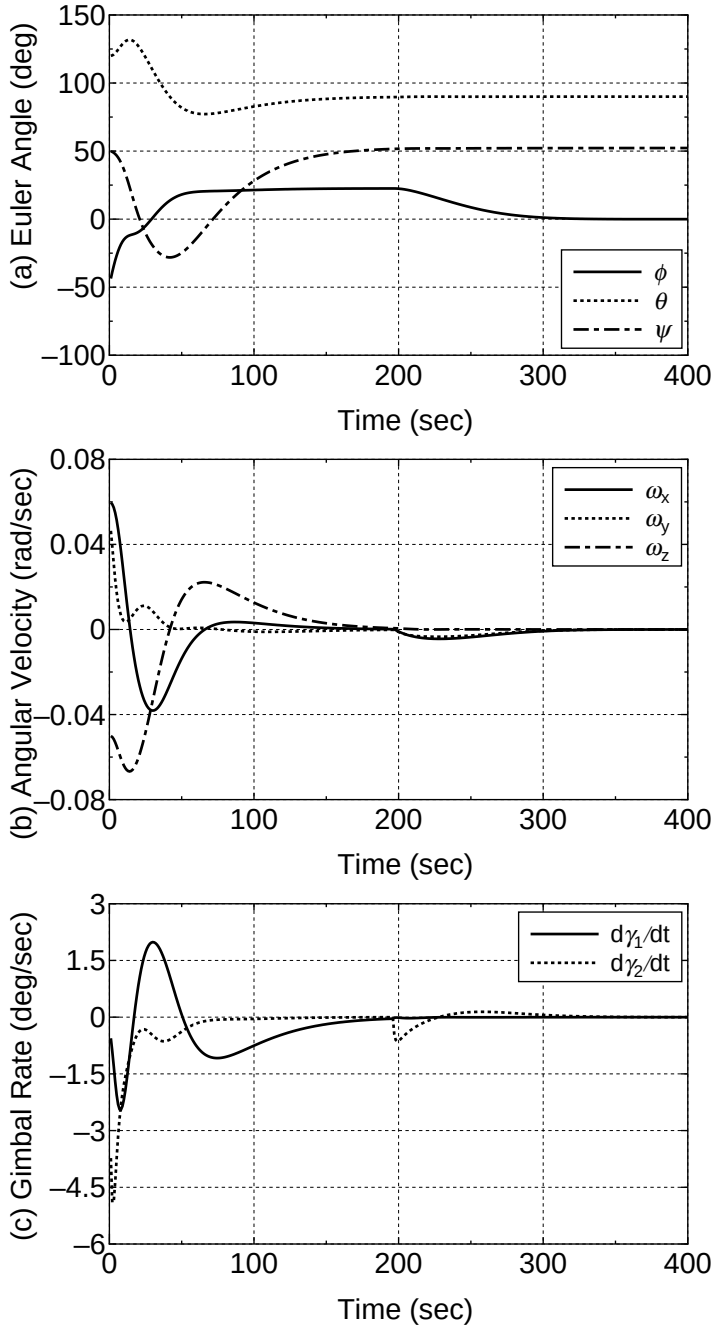

Figure 4.6: Simulation result: **Case 1**

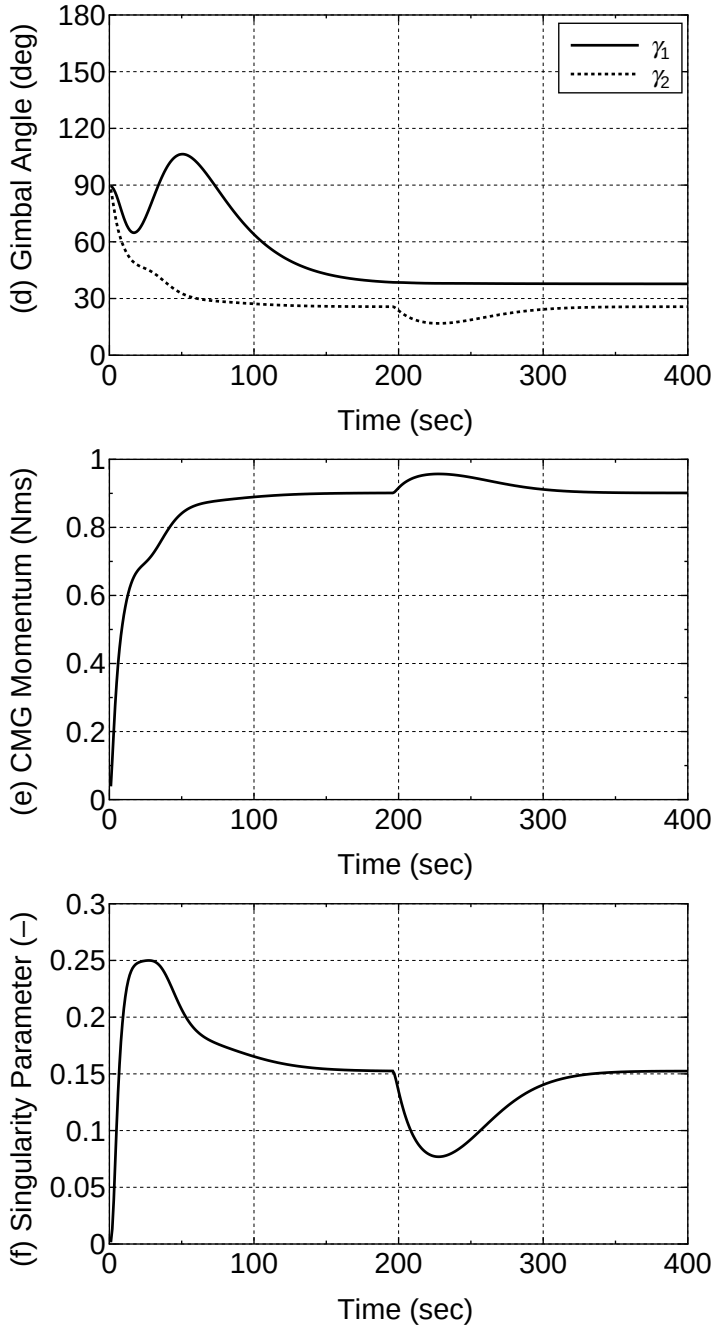

Figure 4.7: Simulation result: **Case 1**

Case 2: Pointing Control to $\hat{n} = [0.6081, 0, -0.7938]^T$

The other desired direction vector for the pointing control is given as $\hat{n} = [0.6081, 0, -0.7938]^T$ in the $\mathcal{F}_H$. Figures 4.8 and 4.9 show the similar results of the numerical simulation, namely, that the variables converge to the right final values, and the pointing control is completed successfully at about 310 sec. In this case, the final Euler angles are given as $\phi_f = 0°$, $\theta_f = 90°$, and $\psi_f = -52.54°$, which gives the final rotation angle as $\gamma_{1f} = 142.54°$.

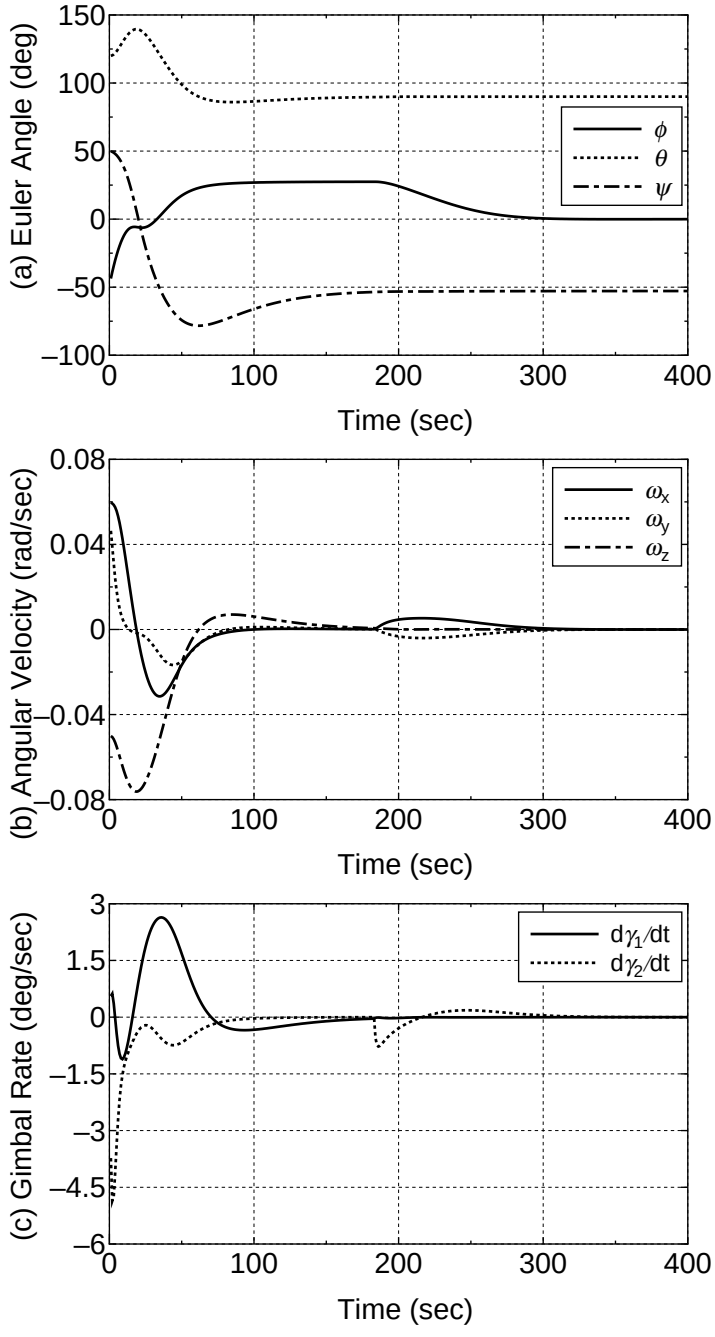

Figure 4.8: Simulation result: **Case 2**

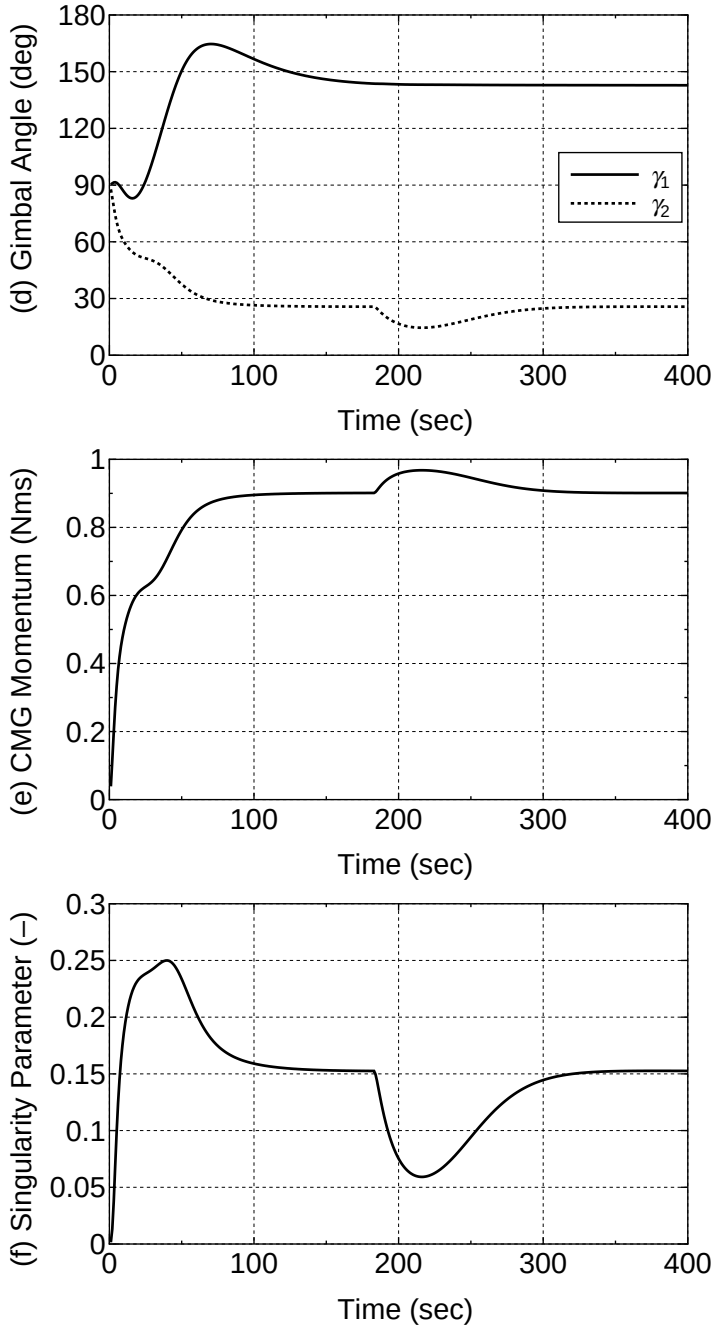

Figure 4.9: Simulation result: **Case 2**

4.6 Conclusion

In this chapter, the author investigated the pointing attitude control of a spacecraft by using a parallel array of two SGCMGs. The feasible orientations of a spacecraft at rest are possible restrictively, because the total angular momentum vector is conserved in the inertial frame.

The author proposed a control strategy which consists of two steps for the pointing control. First, the LQR controller for a linearized system was designed; however, it guaranteed only the local asymptotic stability. Therefore, a nonlinear controller on the basis of the Lyapunov stability theory was proposed for large initial conditions. Finally, the feasibility of the proposed control strategy is validated through numerical simulations.

Chapter 5

Attitude Control of Spacecraft Using SGCMGs via LPV Control Theory

In the previous chapter, we proposed a control strategy which consists of two steps for a pointing control of a spacecraft using two SGCMGs. Even though this two-step strategy effectively worked, it was somehow complicated in both control design and operation since it consists of two steps and needs to switch from one to the other.

In order to provide a one-step strategy which covers a wide operating range of a spacecraft using SGCMGs, in this chapter, we investigate an attitude control of a spacecraft using SGCMGs via Linear Parameter-Varying (LPV) control theory. Based on this theory, nonlinear dynamics of the spacecraft with SGCMGs shall be described as an LPV system and an interesting gain-scheduled (GS) control law is applied to this system. This GS control law consists of extreme controllers designed for each extreme points of the convex hull which covers the operating region of the spacecraft described as an LPV system. The feasibility of the proposed control method is shown by a numerical simulation.

5.1 Preliminary

5.1.1 Linear Matrix Inequality

A linear matrix inequality (LMI) has the form

$$F(x) \triangleq F_0 + x_1 F_1 + x_2 F_2 + \cdots + x_m F_m > 0 \tag{5.1}$$

where $x \in \mathbb{R}^m$ is the variable vector and the symmetric matrices $F_i = F_i^T \in \mathbb{R}^{n \times n}$, $i = 0, \ldots, m$, are given. The inequality symbol in Eq. (5.1) means that F(x) is positive-definite, i.e., $u^T F(x) u > 0$ for all nonzero $u \in \mathbb{R}^n$. Of course, the LMI (5.1) is equivalent to a set of n polynomial inequalities in x, i.e., the leading principal minors of $F(x)$ must be positive.

5.1.2 Linear Parameter-Varying System

Let us consider the Linear Parameter-Varying (LPV) system:

$$\dot{x} = A(\rho)x + Bu + Ew \tag{5.2a}$$

$$z = Cx + Du \tag{5.2b}$$

and the state-feedback gain-scheduled controller:

$$u = -K(\rho)x \tag{5.3}$$

where $x \in \mathbb{R}^n$ is the state vector, $u \in \mathbb{R}^m$ the control input, $w \in \mathbb{R}^{n_w}$ the disturbance input, $z \in \mathbb{R}^{n_z}$ the performance output, and $\rho = [\rho_1, \ldots, \rho_p]$ the scheduling parameter. All the matrices in Eqs. (5.2a) and (5.2b) have appropriate dimensions. Defining $Q = C^T C$ and $R = D^T D$, we assume that

- $R > 0$, $C^T D = 0$
- (A, B): controllable, (C, A): observable.

5.1.3 Matrix Polytope

Let us denote the matrix polytope as follows:

$$M(t) \in \mathrm{Co}\left\{M_1, \ldots, M_p\right\} = \left\{ \sum_{i=1}^{p} \lambda_i M_i : \lambda_i \geq 0, \ \sum_{i=1}^{p} \lambda_i = 1 \right\} \tag{5.4}$$

5.1.4 Lyapunov Function

Using $P > 0$, the Lyapunov function is defined by

$$\mathcal{V} = x^T P x > 0 \tag{5.5}$$

5.1.5 $\mathcal{H}_2$ Performance

For an impulse disturbance w, let us consider the performance index to be minimized:

$$\mathcal{J}_{zw} = \int_0^\infty z^T z \, dt \tag{5.6}$$

which is equivalent to

$$\mathcal{J}_{zw} = \int_0^\infty (x^T Q x + u^T R u) \, dt \tag{5.7}$$

When the closed-loop system is time-invariant, this is identical to the square of the $\mathcal{H}_2$ norm of the closed-loop transfer function from w to z:

$$\mathcal{J}_{zw} = \|H_{zw}(s)\|_2^2 \tag{5.8}$$

When the Lyapunov function is time-varying, minimizing $\mathcal{J}_{zw}$ is equivalent to

$$\inf \quad \text{trace}(E^T P E) \tag{5.9a}$$

$$\text{subject to}$$

$$P > 0, \tag{5.9b}$$

$$\dot{P} + P(A - BK) + (A - BK)^T P + (C - DK)^T (C - DK) < 0 \tag{5.9c}$$

When the Lyapunov function is time-invariant with $\dot{P} = 0$, minimizing $\mathcal{J}_{zw}$ is equivalent to

$$\inf \quad \text{trace}(E^T P E) \tag{5.10a}$$

$$\text{subject to}$$

$$P > 0, \tag{5.10b}$$

$$P(A - BK) + (A - BK)^T P + (C - DK)^T (C - DK) < 0 \tag{5.10c}$$

5.1.6 Schur Complement Formula

The following statements are all equivalent.

$$\begin{bmatrix} \Phi_{11} & \Phi_{12} \\ \Phi_{21} & \Phi_{22} \end{bmatrix} < 0, \tag{5.11a}$$

$$\Phi_{22} < 0, \Phi_{11} - \Phi_{12}\Phi_{22}^{-1}\Phi_{12}^T < 0, \tag{5.11b}$$

$$\Phi_{11} < 0, \Phi_{22} - \Phi_{12}\Phi_{11}^{-1}\Phi_{12}^T < 0 \tag{5.11c}$$

5.1.7 Definition of Matrix Functions

For convenience, let us define the following matrix functions related to $\mathcal{H}_2$ performance. Pre- and postmultiply (5.8) by $X = P^{-1} > 0$ and apply the Schur complement formula, we have

$$\begin{bmatrix} (A - BK)X + \text{sym.} & E \\ * & -I \end{bmatrix} < 0 \tag{5.12}$$

Using the change variables $F \triangleq KX$, Eq. (5.12) is transformed into

$$\begin{bmatrix} AX - BF + \text{sym.} & E \\ * & -I \end{bmatrix} < 0 \tag{5.13}$$

Related to the $\mathcal{H}_2$ objective function, introducing a slack variable Z, we define

$$\begin{bmatrix} Z & CX - DF \\ * & X \end{bmatrix} > 0 \tag{5.14}$$

5.2 Pointing Control of Spacecraft Using Two SGCMGs via LPV Control Theory

In Chapter 4, we consider the pointing control of a spacecraft using two SGCMGs. The control objective for the control problem was stated through the angular momentum conservation principle as follows:

$$\omega \to 0 \tag{5.15a}$$

$$\gamma_{1e} \triangleq \gamma_1 - \gamma_{1f} \to 0 \tag{5.15b}$$

$$\phi_e \triangleq \phi - \phi_f \to 0 \tag{5.15c}$$

where γ_{1e} is the rotation angle error, and ϕ_e is the error of the Euler angle ϕ.

We had proposed a control strategy for the pointing control problem in Chapter 4. The proposed control strategy consists of two steps. In the first step, the control objective (5.15a) and (5.15b) are achieved by using a nonlinear controller on basis of the Lyapunov stability theory. After achieving the control objective (5.15a) and (5.15b), the controller is switched to an LQR controller in the second step to achieve the control objective (5.15c) in addition to (5.15a) and (5.15b). A disadvantage of the proposed control strategy is that the nonlinear controller is necessary for a large initial condition, because the LQR controller guarantees only a local asymptotic stability around an

equilibrium point. As a result, the two-step control strategy described above was required.

In order to provide a one-step control strategy, in the rest of this chapter, we shall develop an interesting GS controller of the spacecraft with two SGCMGs described as an LPV system.

5.2.1 LPV System Modeling of Spacecraft with Two SGCMGs

First, the nonlinear system of a spacecraft with two SGCMGs can be expressed as

$$\dot{\omega} = -J^{-1}\omega^{\times}(J\omega + h(\gamma)) - J^{-1}G(\gamma)\dot{\gamma} \tag{5.16}$$

where the spacecraft angular velocity vector $\omega \in \mathbb{R}^3$ is the state vector, the gimbal rate vector $\dot{\gamma} \in \mathbb{R}^2$ is the control input vector, and the gimbal angle vector $\gamma \in \mathbb{R}^2$ is the scheduling parameter vector. The Jacobian linearization of Eq. (5.16) around the equilibrium point ($\omega_{eq} = 0,\ \dot{\gamma}_{eq} = 0$) leads as follows:

$$\left.\frac{\partial\dot{\omega}}{\partial\omega}\right|_{\omega_{eq},\dot{\gamma}_{eq}} = J^{-1}h(\gamma)^{\times} \tag{5.17a}$$

$$\left.\frac{\partial\dot{\omega}}{\partial\dot{\gamma}}\right|_{\omega_{eq},\dot{\gamma}_{eq}} = -J^{-1}G(\gamma) \tag{5.17b}$$

Thus, we can be obtained as following system:

$$\dot{\omega} = J^{-1}h(\gamma)^{\times}\omega - J^{-1}G(\gamma)\dot{\gamma} \tag{5.18}$$

Next, the differential equation of the rotation angle error γ_{1e} is given by

$$\dot{\gamma}_{1e} = \dot{\gamma}_1 \tag{5.19}$$

Finally, from Eq. (4.6), the differential equation of the Euler angle error ϕ_e is given by

$$\dot{\phi}_e = \dot{\phi} = [\sin\psi\,\mathrm{cosec}\,\theta,\ \cos\psi\,\mathrm{cosec}\,\theta,\ 0]\omega \tag{5.20}$$

For ease of analysis, we apply the relation of $\theta_f = 90^\circ$ and $\gamma_{1f} = 90^\circ - \psi_f$ to Eq. (5.20) Assuming that $\mathrm{cosec}\,\theta \approx 1$ and $\psi \approx 90^\circ - \gamma_1$ around the final values, Eq. (5.20) is rewritten as follows:

$$\dot{\phi}_e \approx [\cos\gamma_1,\ \sin\gamma_1,\ 0]\omega \triangleq M(\gamma)\omega \tag{5.21}$$

Therefore, we can obtain the following system with the state vector $x_p = [\omega^T,\ \gamma_{1e},\ \phi_e]^T \in \mathbb{R}^5$ as follows:

$$\dot{x}_p = A_r(\gamma)x_p + B_r(\gamma)\dot{\gamma} \tag{5.22}$$

where:

$$A_r = \begin{bmatrix} J^{-1}h(\gamma)^\times & 0 & 0 \\ 0 & 0 & 0 \\ M(\gamma) & 0 & 0 \end{bmatrix}\begin{bmatrix} \omega \\ \gamma_{1e} \\ \phi_e \end{bmatrix},\ B_r = \begin{bmatrix} -J^{-1}g_1(\gamma) & -J^{-1}g_2(\gamma) \\ 1 & 0 \\ 0 & 0 \end{bmatrix}$$

where $g_i(\gamma)$, for $i = 1,\ 2$ is the ith column vector of the matrix $G(\gamma)$. However, the elements of system matrices $A_r(\gamma)$ and $B_r(\gamma)$ are trigonometric functions of γ; see Appendix A and this system has not been yet an LPV system. In order to convert this system into an LPV system, let us define a new scheduling parameter $\rho \in \mathbb{R}^4$ as follows:

$$\rho_1 \triangleq \sin\gamma_1,\ \rho_2 \triangleq \sin\gamma_2,\ \rho_3 \triangleq \cos\gamma_1,\ \rho_4 \triangleq \cos\gamma_2 \tag{5.23}$$

It should be noted that $\rho_i \in [-1,\ 1]$, $i = 1, \ldots, 4$. Using the new scheduling parameter ρ, the system of Eq. (5.22) can be converted into the LPV system described as

$$\dot{x}_p = A_p(\rho)x_p + B_p(\rho)\dot{\gamma} \tag{5.24}$$

where:

$$A_p(\rho) = \begin{bmatrix} J^{-1}h(\rho)^\times & 0 & 0 \\ 0 & 0 & 0 \\ M(\rho) & 0 & 0 \end{bmatrix},\ B_p(\rho) = \begin{bmatrix} -J^{-1}g_1(\rho) & -J^{-1}g_2(\rho) \\ 1 & 0 \\ 0 & 0 \end{bmatrix}$$

The readers might be in doubt that matrices $A_p(\rho)$ and $B_p(\rho)$ include the product $\rho_i\rho_j$, $i = 1,\ 3$, $j = 2,\ 4$ in addition to the elements of ρ_i, $i = 1,\ 3$ alone, and the system in Eq. (5.24) has not been yet an LPV system. However, the range of the value of $\rho_i\rho_j$, $i = 1,\ 3$, $j = 2,\ 4$ is included in that of ρ_j, $j = 2,\ 4$, while depending on the sign of ρ_i, $i = 1,\ 3$. Taking account of this feature, we can construct a convex hull which covers the operating range of the system in Eq. (5.24) and take its extreme points or vertices as if it were an LPV system which linearly depends on ρ_i, $i = 1, \ldots, 4$. Although the system in Eq. (5.24) is not an LPV system in a strict sense, we shall regard it as an LPV system in the sequel from the reason described above.

Note that the control input matrix depends on the ρ. Since this type of LPV system does not satisfy the condition that the control input matrix is parameter-independent, it is difficult to design a GS controller on basis of LMIs [1]. However, this problem

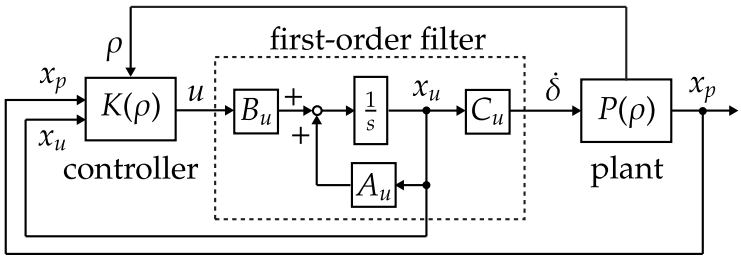

Figure 5.1: The block diagram of the first-order filter

can be solve by inserting a first-order filter as shown in Fig. 5.1. Define a new control input vector $u \in \mathbb{R}^2$ by

$$\dot{x}_u = A_u x_u + B_u u \tag{5.25a}$$

$$\dot{\gamma} = C_u x_u \tag{5.25b}$$

where coefficient matrices $A_u \in \mathbb{R}^{2\times2}$, $B_u \in \mathbb{R}^{2\times2}$, and $C_u \in \mathbb{R}^{2\times2}$ are the design parameters of the filter.

From Eqs. (5.24) and (5.25), defining the new state vector $x = [x_p^T,\ x_u^T]^T$, the augmented system can be given by

$$\dot{x} = A(\rho)x + Bu \tag{5.26}$$

where:

$$A(\rho) = \begin{bmatrix} A_p(\rho) & B_p C_u \\ 0 & A_u \end{bmatrix},\ B = \begin{bmatrix} 0 \\ B_u \end{bmatrix}$$

Note that the control input matrix is independent from the scheduling parameter vector ρ.

5.2.2 Design of GS Controller

Now let us introduce the disturbance input vector $w \in \mathbb{R}^4$ and the performance output vector $z \in \mathbb{R}^9$. The former takes account of model errors, while the latter represents the control performance for the disturbance repression. With the the disturbance input vector and the performance output vector, the LPV system can be expanded as

$$\dot{x} = A(\rho)x + Bu + Ew \tag{5.27a}$$

$$z = Cx + Du \tag{5.27b}$$

where $x = [x_p^T,\ x_u^T]^T \in \mathbb{R}^7$ is the state vector, the coefficient matrices $C \in \mathbb{R}^{9\times7}$ and $D \in \mathbb{R}^{9\times2}$ satisfy $C^TD = 0$, $D^TD > 0$ and $E \in \mathbb{R}^{7\times4}$. To this LPV system, we develop the sate-feedback gain-scheduled (GS) controller:

$$u = -K(\rho)x \tag{5.28}$$

The closed-loop system of the LPV system in Eqs. (5.27a), (5.27b) with the GS controller in Eq. (5.28) is stable and is guaranteed $\mathcal{H}_2$ performance if there exists a matrix X which satisfies the following LMI:

$$\inf_{\rho, X, Z} \quad \text{trace } Z \tag{5.29a}$$

$$\text{subject to}$$

$$\begin{bmatrix} Z & CX - DF(\rho) \\ * & X \end{bmatrix} > 0, \tag{5.29b}$$

$$\begin{bmatrix} A(\rho)X - BF(\rho) + \text{sym.} & E \\ * & -I \end{bmatrix} < 0 \tag{5.29c}$$

where $F(\rho) = K(\rho)X$. The scheduling parameter vector $\rho \in \mathbb{R}^4$ has $2^4 = 16$ vertices. Setting $p = 16$ as the number of the vertices, the LPV system can be expressed by the following polytopic representation:

$$A(\rho) = \sum_{i=1}^{p} \lambda_i(\rho) A_i \tag{5.30a}$$

$$K(\rho) = \sum_{i=1}^{p} \lambda_i(\rho) K_i \tag{5.30b}$$

$$F(\rho) = \sum_{i=1}^{p} \lambda_i(\rho) F_i \tag{5.30c}$$

where:

$$\sum_{i=1}^{p} \lambda_i(\rho) = 1, \quad \lambda_i(\rho) \geq 0 \tag{5.31}$$

The LMIs in Eq. (5.29a) - (5.29c) can be rewritten as

$$\inf_{F_i, X, Z} \ \text{trace}\ Z \tag{5.32a}$$

subject to

$$\begin{bmatrix} Z & CX - DF_i \\ * & X \end{bmatrix} > 0, \tag{5.32b}$$

$$\begin{bmatrix} A_iX - BF_i + \text{sym.} & E \\ * & -I \end{bmatrix} < 0 \tag{5.32c}$$

Using the optimal solution sets (F_i, X), extreme controllers are given by $K_i = F_iX^{-1}$, $i = 1, \ldots, p$ and a GS controller is constructed as follows:

$$K(\rho) = \sum_{i=1}^{p} \lambda_i K_i \tag{5.33}$$

In this case, the GS controller is determined by the common Lyapunov solution $X > 0$ and tends to result in conservatism.

As an alternative method, we can consider another problem, in which distinct Lyapunov solutions $X_i > 0$, $i = 1, \ldots, p$ are adopted [19]:

$$\inf_{F_i, X_i, Z_i} \ \text{trace}\ Z_i \tag{5.34a}$$

subject to

$$\begin{bmatrix} Z_i & CX_i - DF_i \\ * & X_i \end{bmatrix} > 0, \tag{5.34b}$$

$$\begin{bmatrix} A_iX_i - BF_i + \text{sym.} & E \\ * & -I \end{bmatrix} < 0 \tag{5.34c}$$

Using the optimal solution sets (F_i, X_i), extreme controllers are given by $K_i = F_iX_i^{-1}$, $i = 1, \ldots, p$ and a GS controller in constructed as in Eq. (5.33).

In this case, in order to guarantee the overall stability of the closed-loop system for a whole operating range, we need to check the feasibility of the following inequality:

$$\exists P > 0, \ \ P(A_i - BK_i) + (A_i - BK_i)^T P < 0, \ \ \forall i \tag{5.35}$$

after obtaining the extreme controllers K_i, $i = 1, \ldots, p$. This alternative method leads to a less conservative design result which improves the control performance in many cases [19].

Table 5.1: Parameters of the spacecraft model and initial condition

Symbol	Value	Units
J	diag[10, 10, 9]	kgm^2
h_w	0.5	Nms
ω_0	$[0.06,\ 0.05,\ -0.05]^T$	rad/sec
γ_0	$[90,\ 90]^T$	deg
$\dot{\gamma}_0$	$[0,\ 0]^T$	deg/sec

Table 5.2: Design parameters of the controller and filter

Symbol	Value	Units
A_u	diag$[-1,\ -1]$	–
B_u	diag[0.1, 0.1]	–
C_u	diag[2, 2]	–
C	see Appendix B	–
D	see Appendix B	–
E	see Appendix B	–

5.2.3 Numerical Simulation A

In this subsection, we present a numerical simulation result of the pointing control problem by using the proposed GS controller. The parameters of the spacecraft model with two SGCMGs and the initial condition used for the simulation are given in Table 5.1. The design parameters of the controller and the filter are given in Table 5.2.

Case 1: Pointing Control to $\hat{n} = [0.6081\ , 0, 0.7938]^T$

In this case, we give a desired direction vector $\hat{n} = [0.6081\ , 0, 0.7938]^T$ in the $\mathcal{F}_H$. The simulation results are shown in Figs. 5.2 and 5.3, in which (a) the Euler angle; (b) the spacecraft angular velocity; (c) the gimbal rate; (d) the gimbal angle; (e) the CMG angular momentum; and (f) the singularity parameter (i.e. $\det(G^T G)$) are given. As shown in Fig. 5.2(a), the Euler angles ϕ, θ, and ψ converge to the final values as $\phi_f = 0°$, $\theta_f = 90°$, and $\psi_f = 52.54°$ almost within 120 sec, respectively, while the spacecraft angular velocity ω converges to zero after about 120 sec as shown in Fig. 5.2(b). Figure 5.3(d) shows the rotation angle γ_1 converges to $\gamma_{1f} = 37.46°$ $(90° - \psi_f)$.

The GS controller is effectively worked than the proposed two step strategy in Chapter 4.

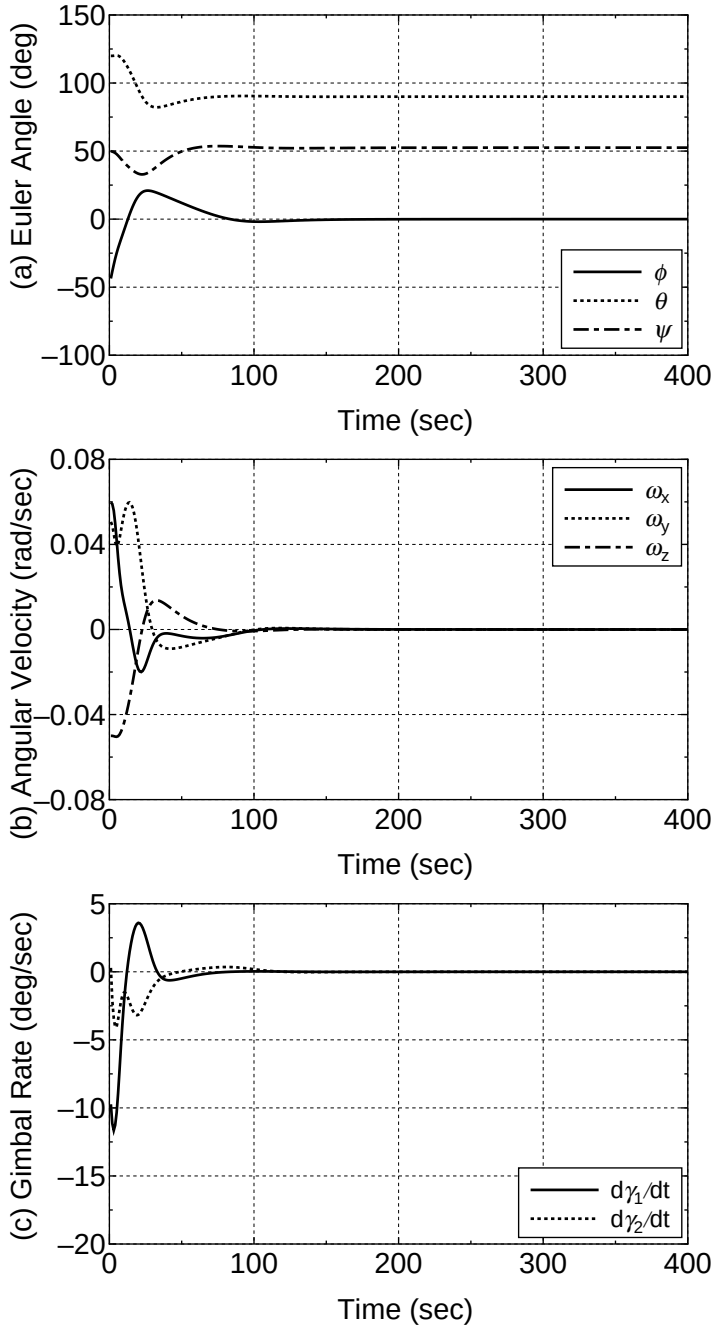

Figure 5.2: Simulation result: **Case 1** (GS controller)

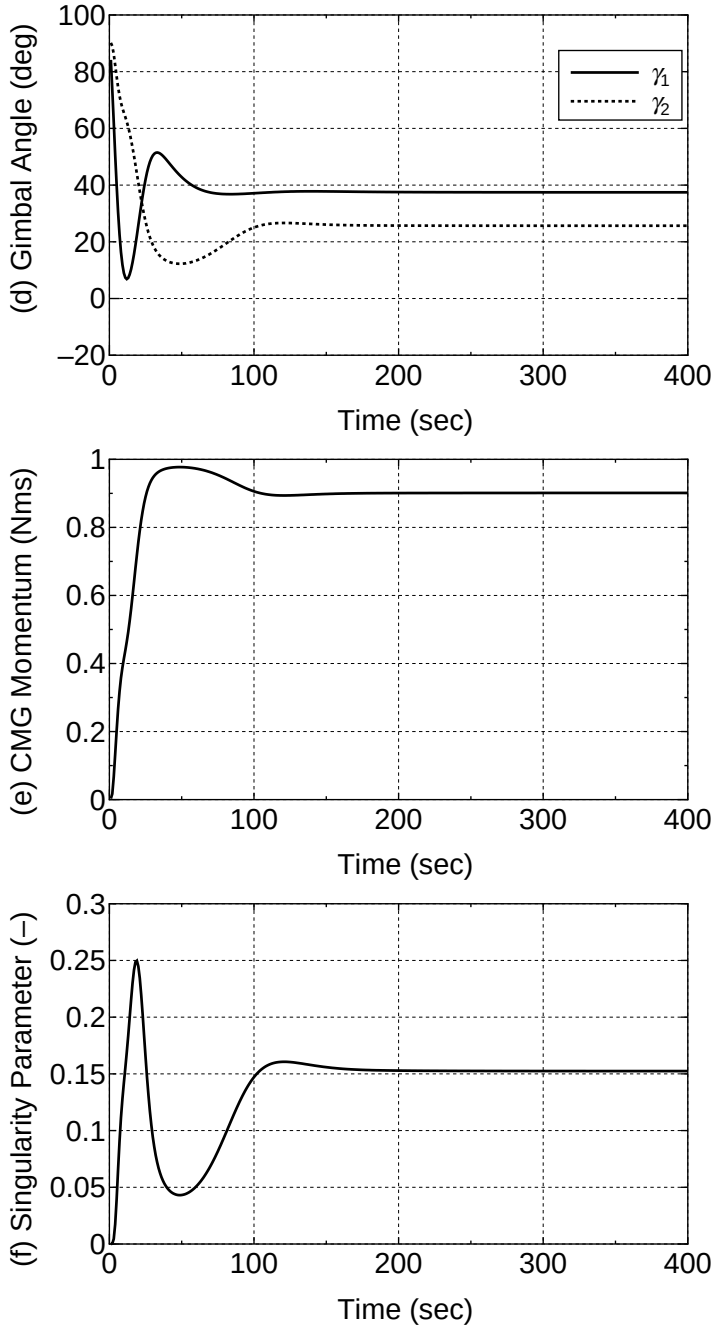

Figure 5.3: Simulation result: **Case 1** (GS controller)

Case 2: Pointing Control to $\hat{n} = [0.3595,\ 0,\ 2.9784]^T$

The other desired direction vector is given as $\hat{n} = [0.3595,\ 0,\ 2.9784]^T$ in the $\mathcal{F}_H$. In this case, the final Euler angles are given as $\phi_f = 0°$, $\theta_f = 90°$, and $\psi_f = 83.12°$. The final rotation angle is given as $\gamma_{1f} = 6.88°$. Again, almost similar result can be seen as shown in Figs. 5.4 and 5.5.

At about 25 sec, the singularity of $\gamma_2 = 0°$ is encountered as shown in Fig. 5.5(d). It can be shown that the angular momentum vectors of two SGCMGs are corresponding. Therefore, the norm of the CMG angular momentum becomes the maximum value, $\|h\|_{max} = 1$ as shown in Fig. 5.5(e). In Fig. 5.5(f), the singularity parameter $\det(G^T G)$ becomes zero. In this case, the settling time is about 220 sec.

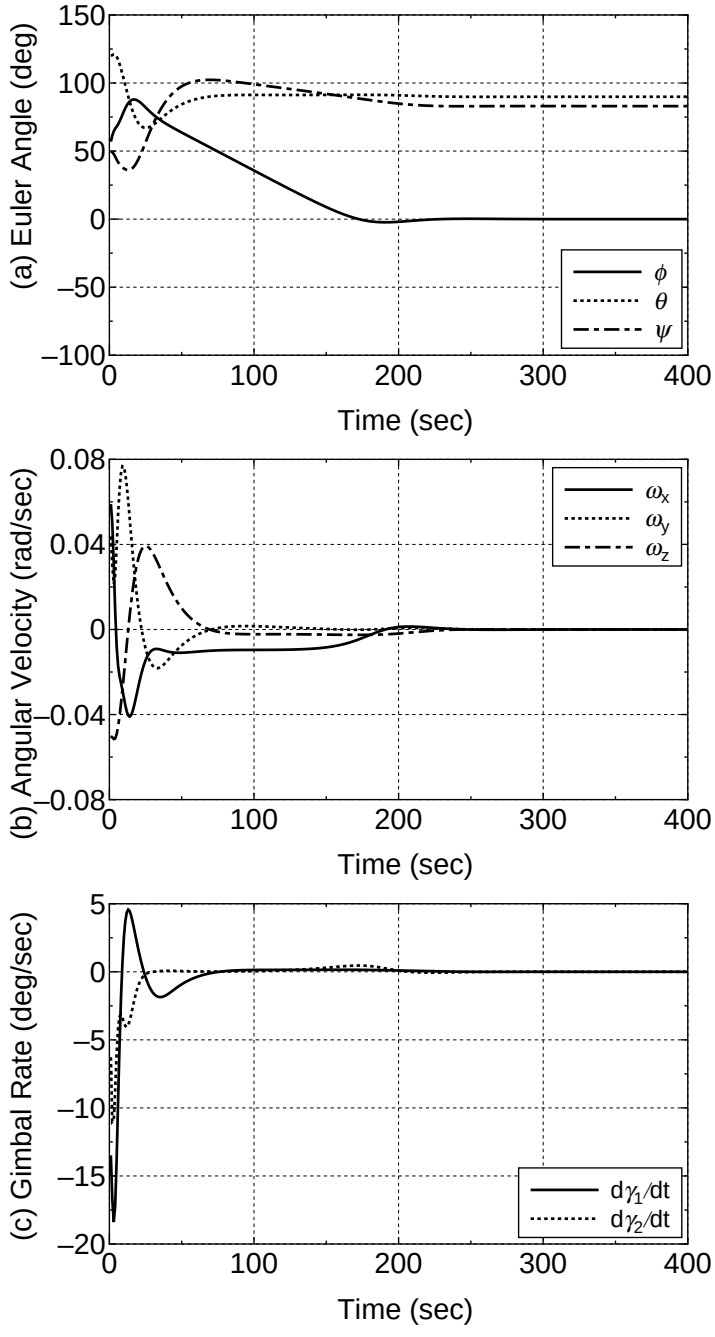

Figure 5.4: Simulation result: **Case 2** (GS controller)

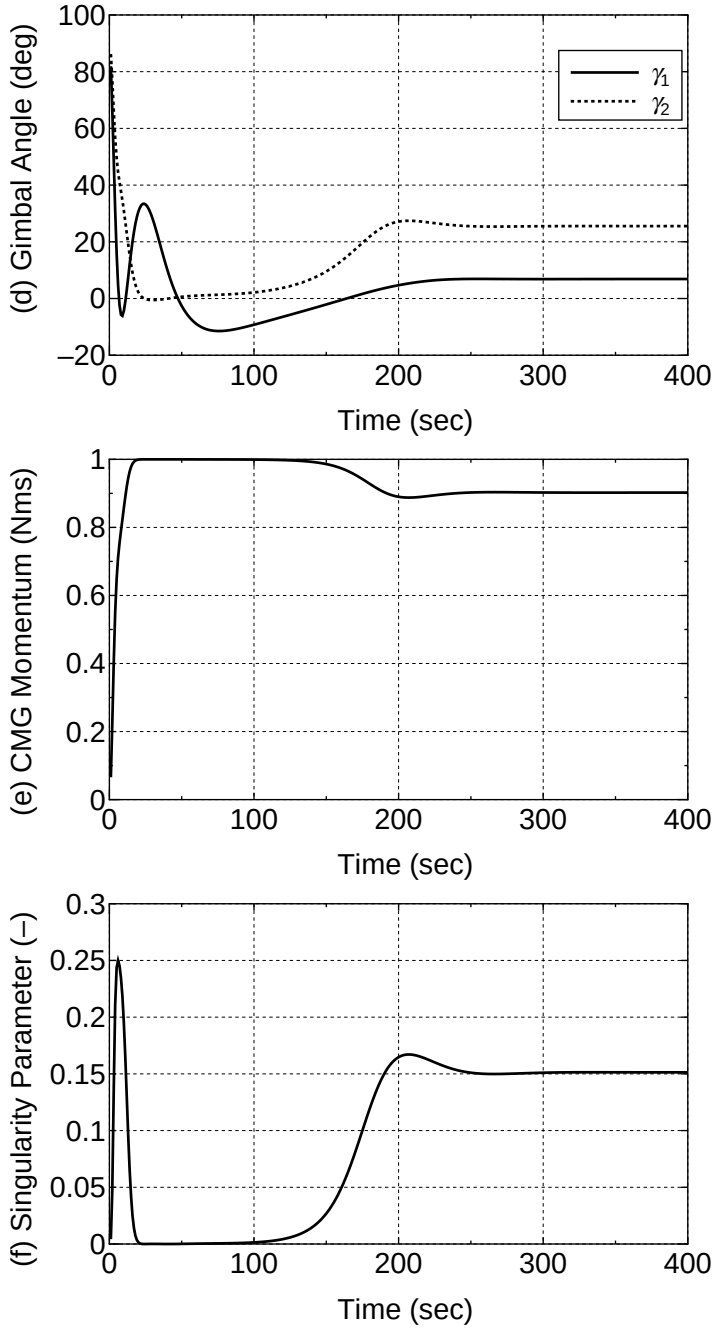

Figure 5.5: Simulation result: **Case 2** (GS controller)

5.3 Attitude Control of Spacecraft Using Four SGCMGs via LPV Control Theory

In this section, we consider the general maneuvers using four SGCMGs. After the LPV modeling of a spacecraft with four SGCMGs, the control performances of a simple LQR controller and the proposed GS controller in the previous section are compared through numerical simulation.

5.3.1 LPV System Modeling of Spacecraft with Four SGCMGs

From Eqs. (2.15) and (2.7), the dynamical equation of a spacecraft with an SGCMG cluster and the kinematic differential equation of the MRPs are given by

$$\dot{\omega} = -J^{-1}\omega^{\times}(J\omega + h(\delta)) - J^{-1}G(\delta)\dot{\delta} \tag{5.36a}$$

$$\dot{\sigma} = \frac{1}{2}\left(\frac{1}{2}(1-\sigma^T\sigma)I_{3\times 3} + \sigma^{\times} + \sigma\sigma^T\right)\omega \tag{5.36b}$$

In this chapter, a standard four SGCMGs pyramid configuration shown in Fig. 3.1 is used. Thus, the angular momentum $h(\delta) \in \mathbb{R}^3$ is

$$h(\delta) = h_w \begin{bmatrix} -c\beta\sin\delta_1 - \cos\delta_2 + c\beta\sin\delta_3 + \cos\delta_4 \\ \cos\delta_1 - c\beta\sin\delta_2 - \cos\delta_3 + c\beta\sin\delta_4 \\ s\beta\sin\delta_1 + s\beta\sin\delta_2 + s\beta\sin\delta_3 + s\beta\sin\delta_4 \end{bmatrix} \tag{5.37}$$

where h_w is the magnitude of the angular momentum of a wheel, $s\beta = \sin\beta$ and $c\beta = \cos\beta$. The Jacobian matrix $G(\delta) \in \mathbb{R}^{3\times 3}$ is given by

$$G(\delta) = h_w \begin{bmatrix} -c\beta\cos\delta_1 & \sin\delta_2 & c\beta\cos\delta_3 & -\sin\delta_4 \\ -\sin\delta_1 & -c\beta\cos\delta_2 & \sin\delta_3 & c\beta\cos\delta_4 \\ s\beta\cos\delta_1 & s\beta\cos\delta_2 & s\beta\cos\delta_3 & s\beta\cos\delta_4 \end{bmatrix} \tag{5.38}$$

The Jacobian linearization of Eqs. (5.36a) and (5.36b) around the equilibrium point leads as follows:

$$\left.\frac{\partial\dot{\omega}}{\partial\omega}\right|_{\omega_{eq},\dot{\delta}_{eq}} = J^{-1}h(\delta)^{\times} \tag{5.39a}$$

$$\left.\frac{\partial\dot{\omega}}{\partial\dot{\delta}}\right|_{\omega_{eq},\dot{\delta}_{eq}} = -J^{-1}G(\delta) \tag{5.39b}$$

$$\left.\frac{\partial\dot{\sigma}}{\partial\omega}\right|_{\omega_{eq},\sigma_{eq}} = \frac{1}{4}I_{3\times 3} \tag{5.39c}$$

$$\left.\frac{\partial\dot{\sigma}}{\partial\sigma}\right|_{\omega_{eq},\sigma_{eq}} = 0 \tag{5.39d}$$

Therefore, we can obtain the following system:

$$\begin{bmatrix} \dot{\omega} \\ \dot{\sigma} \end{bmatrix} = \begin{bmatrix} J^{-1}h(\delta)^{\times} & 0 \\ \frac{1}{4}I_{3\times 3} & 0 \end{bmatrix} \begin{bmatrix} \omega \\ \sigma \end{bmatrix} + \begin{bmatrix} -J^{-1}G(\delta) \\ 0 \end{bmatrix} \dot{\delta} \tag{5.40}$$

However, the elements of system matrix and control input matrix are trigonometric functions of δ and this system has not been yet an LPV system. In order to convert this system into an LPV system, let us define a new scheduling parameter $\rho \in \mathbb{R}^4$ as follows:

$$\rho_1 \triangleq \sin\delta_1,\ \rho_2 \triangleq \sin\delta_2,\ \rho_3 \triangleq \sin\delta_3,\ \rho_4 \triangleq \sin\delta_4 \tag{5.41}$$

It should be noted that $\rho_i \in [-1,\ 1]$, $i = 1, \ldots, 4$. In addition, we linearize as follows:

$$\cos\delta_1 \approx 1,\ \ \cos\delta_2 \approx 1,\ \ \cos\delta_3 \approx 1,\ \ \cos\delta_4 \approx 1 \tag{5.42}$$

Using the new scheduling parameter ρ, the above system can be converted into the LPV system described as

$$\begin{bmatrix} \dot{\omega} \\ \dot{\sigma} \end{bmatrix} = \begin{bmatrix} J^{-1}h(\rho)^{\times} & 0 \\ \frac{1}{4}I_{3\times 3} & 0 \end{bmatrix} \begin{bmatrix} \omega \\ \sigma \end{bmatrix} + \begin{bmatrix} -J^{-1}G(\rho) \\ 0 \end{bmatrix} \dot{\delta} \tag{5.43}$$

Note that the control input matrix depends on the ρ. Since this type of LPV system does not satisfy the condition that the control input matrix is parameter-independent, it is difficult to design a GS controller on basis of LMIs [1]. However, this problem can be solve by inserting a first-order filter as shown in Fig. 5.1. Define a new control input vector u by

$$\dot{x}_u = A_u x_u + B_u u \tag{5.44a}$$

$$\dot{\delta} = C_u x_u \tag{5.44b}$$

where coefficient matrices $A_u \in \mathbb{R}^{4\times 4}$, $B_u \in \mathbb{R}^{4\times 4}$, and $C_u \in \mathbb{R}^{4\times 4}$ are the design parameters of the filter. From Eqs. (5.43), (5.44a) and (5.44b), defining the new state vector $x = [\omega^T, \sigma^T, x_u^T]^T \in \mathbb{R}^{10}$, the augmented system can be given by

$$\dot{x} = A(\rho)x + Bu \tag{5.45}$$

where:

$$A(\rho) = \begin{bmatrix} J^{-1}h(\rho)^{\times} & 0 & -J^{-1}G(\rho)C_u \\ \frac{1}{4}I_{3\times 3} & 0 & 0 \\ 0 & 0 & A_u \end{bmatrix},\ B = \begin{bmatrix} 0 \\ 0 \\ B_u \end{bmatrix} \tag{5.46}$$

Note that the control input matrix is independent from the scheduling parameter vector ρ.

Table 5.3: Parameters of the spacecraft model and initial condition

Symbol	Value	Units
J	diag[10, 10, 9]	kgm^2
h_w	0.5	Nms
β	54.73	deg
ω_0	$[0,\ 0,\ 0]^T$	rad/sec
δ_0	$[0,\ 0,\ 0,\ 0]^T$	deg
$\dot{\delta}_0$	$[0,\ 0,\ 0,\ 0]^T$	rad/sec

Table 5.4: Design parameters of the controller and filter

Symbol	Value	Units
Q	diag[10^3, 10^3, 10^3, 10^5, 10^5, 10^5]	–
R	diag[10^6, 10^6, 10^6, 10^6]	–
A_u	diag[-10, -10, -10, -10]	–
B_u	diag[8, 8, 8, 8]	–
C_u	diag[7, 7, 7, 7]	–
C	see Appendix B	–
D	see Appendix B	–
E	see Appendix B	–

5.3.2 Numerical Simulation B

In this subsection, we present a numerical simulation result of the attitude control by using the proposed GS controller in Subsection 5.2.2. In order to compare, the result by using LQR controller also is presented. The parameters of the spacecraft model with four SGCMGs and the initial condition used for the simulation are given in Table 5.3. The design parameters of the controller and filter are given in Table 5.4.

Case 1: Three-Axis Maneuver

In this case, we give a initial condition of $\sigma_0 = [1/3, -1/3, -1/3]^T$. A simulation result of the maneuver using the LQR controller is shown in Figs. 5.6 and 5.7, and that with the proposed GS controller is shown in Figs. 5.8 and 5.9. In Figs. 5.6 - 5.9, (a) shown the MRPs; (b) the Euler angle; (c) the spacecraft angular velocity; (d) the gimbal rate; (e) the gimbal angle; and (f) the CMG angular momentum.

As shown in Fig. 5.6(a), the maneuver using LQR controller is completed in about 125 sec, whereas the maneuver using proposed GS controller is finished in about 80 sec as shown in Fig. 5.8(a).

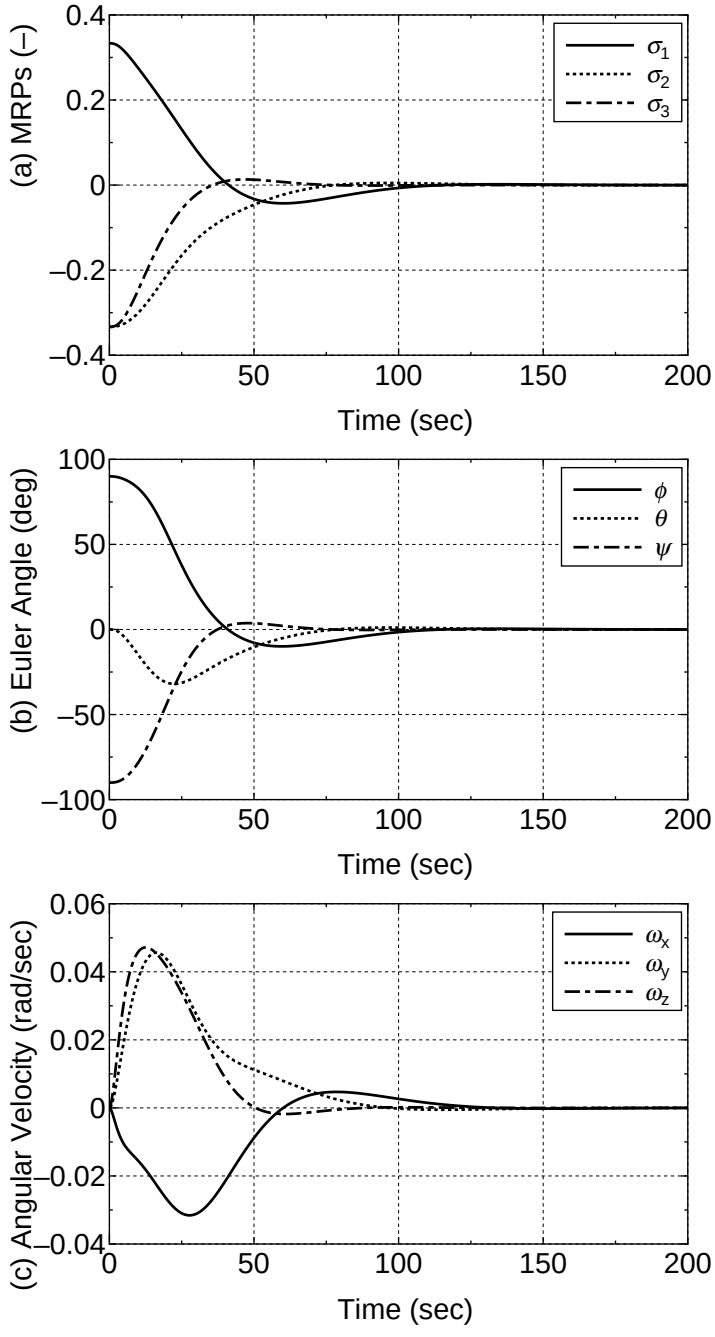

Figure 5.6: Simulation result: **Case 1** (LQR controller)

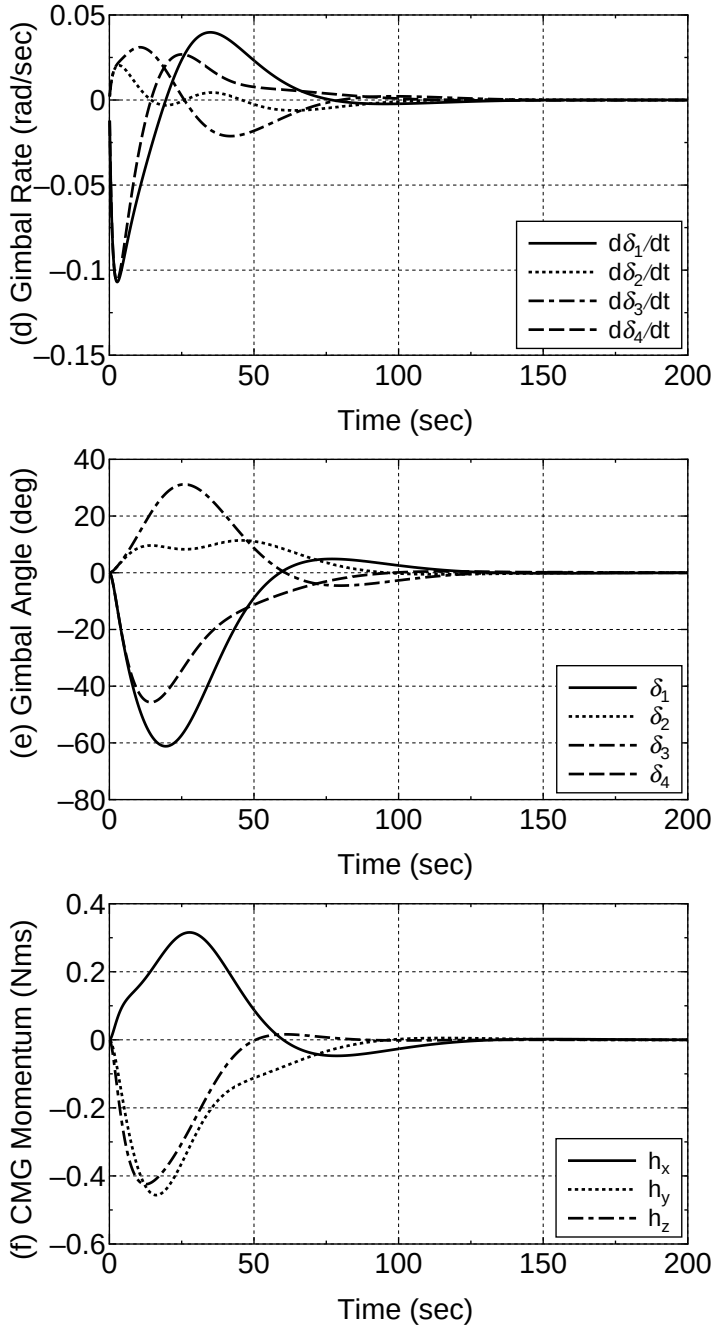

Figure 5.7: Simulation result: **Case 1** (LQR controller)

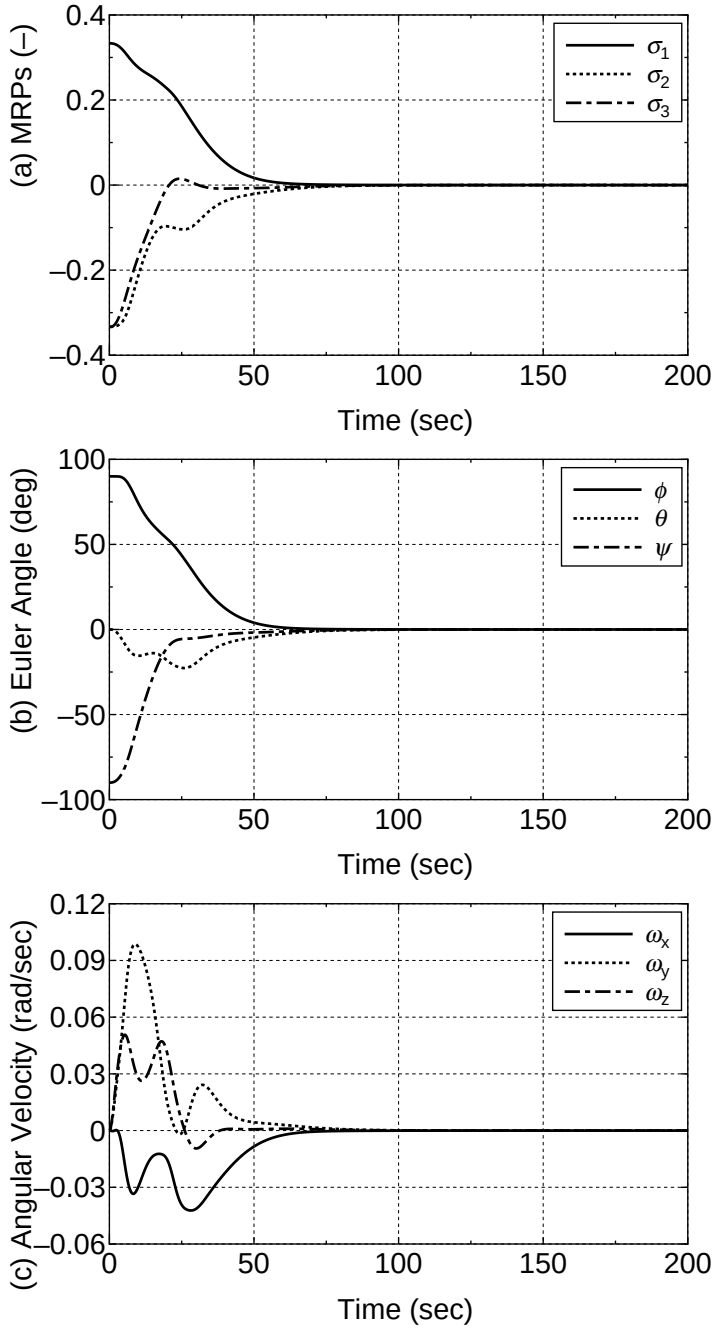

Figure 5.8: Simulation result: **Case 1** (GS controller)

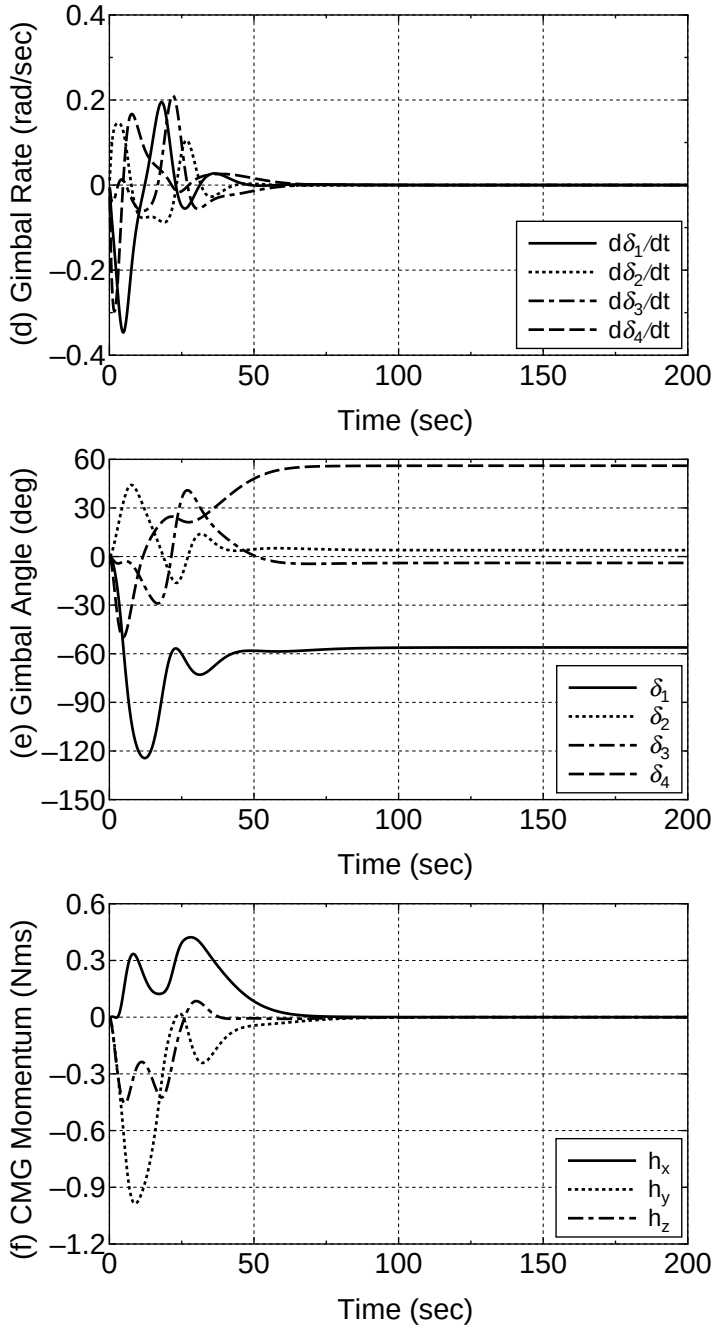

Figure 5.9: Simulation result: **Case 1** (GS controller)

Case 2: Large-Angle Maneuver

In this case, we give the other initial condition of $\sigma_0 = [1, 0, 0]^T$. This maneuver is the large-angle maneuver of 180 degrees around x axis. A simulation result of the maneuver using the LQR controller is shown in Figs. 5.10 and 5.11, and that with the proposed GS controller is shown in Figs. 5.12 and 5.13. In Figs. 5.10 - 5.13, (a) shown the MRPs; (b) the Euler angle; (c) the spacecraft angular velocity; (d) the gimbal rate; (e) the gimbal angle; and (f) the CMG angular momentum.

By using the LQR controller, the large-angle maneuver is completed in about 170 sec as shown in Figs. 5.10(a) and (b). To generate output torque about x axis, only 1st and 3rd SGCMGs are operated during the maneuver as shown Figs. 5.11(d) and (e).

On the other hand, Figs. 5.12(a) and (b) shows that the maneuver using the proposed GS controller is completed in about 120 sec. All SGCMGs are actively operated as shown Figs. 5.13(d) and (e).

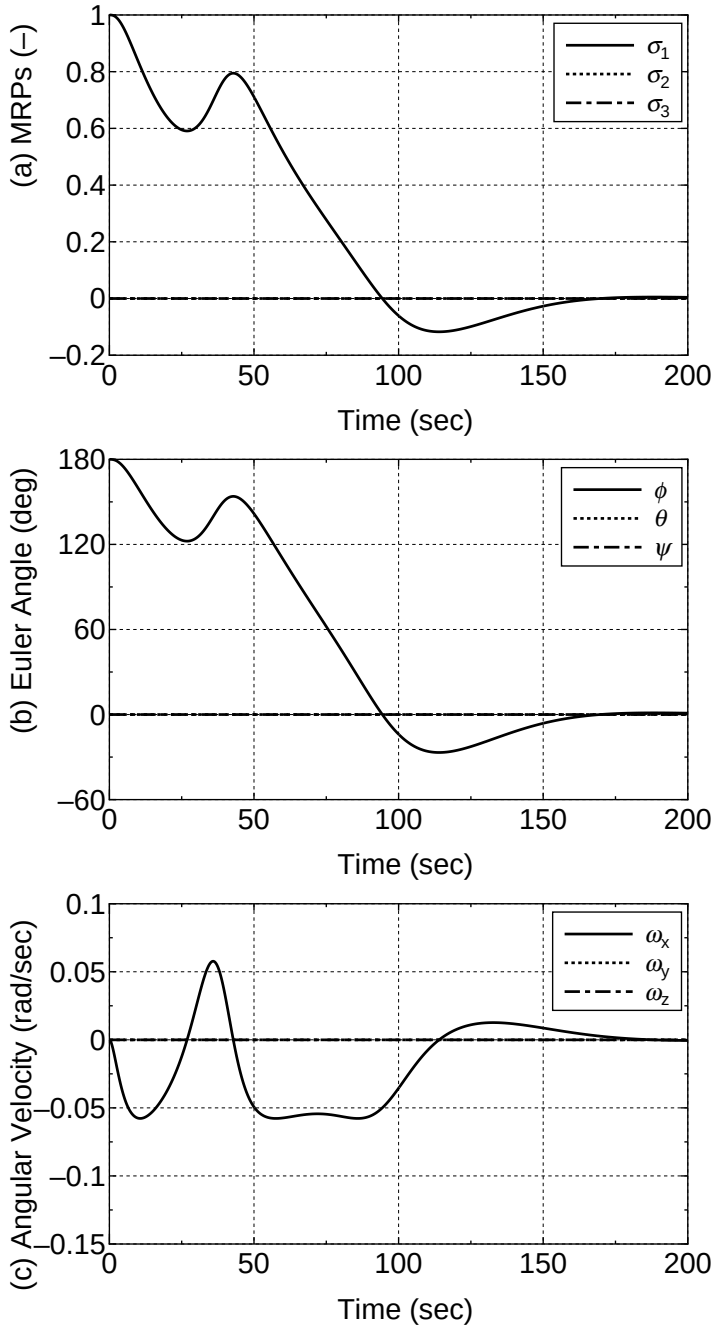

Figure 5.10: Simulation result: **Case 2** (LQR controller)

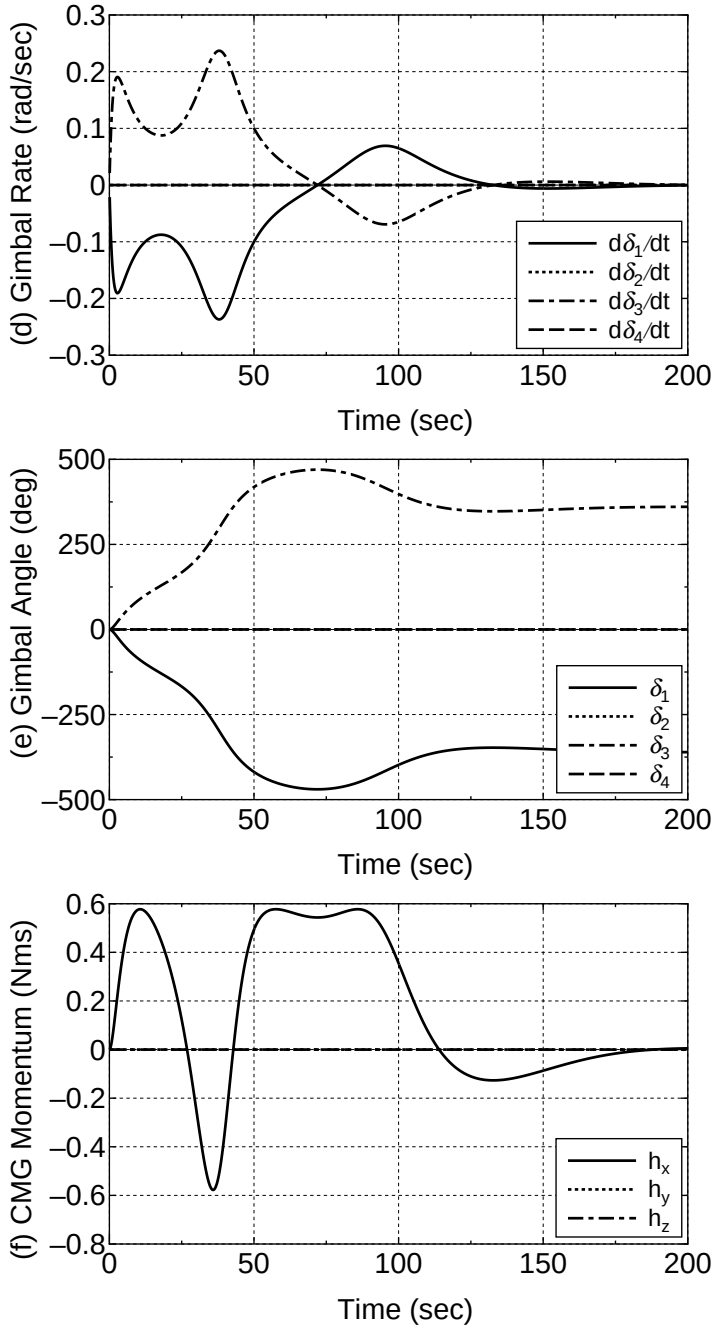

Figure 5.11: Simulation result: **Case 2** (LQR controller)

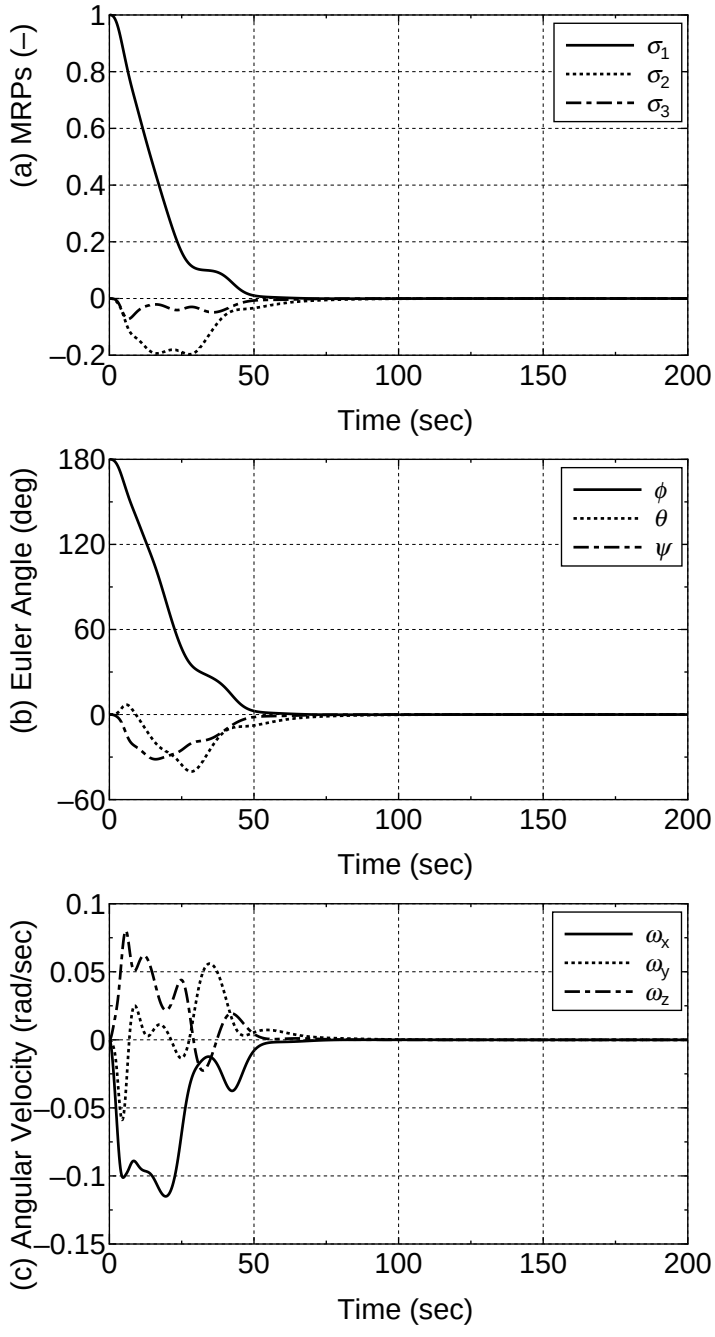

Figure 5.12: Simulation result: **Case 2** (GS controller)

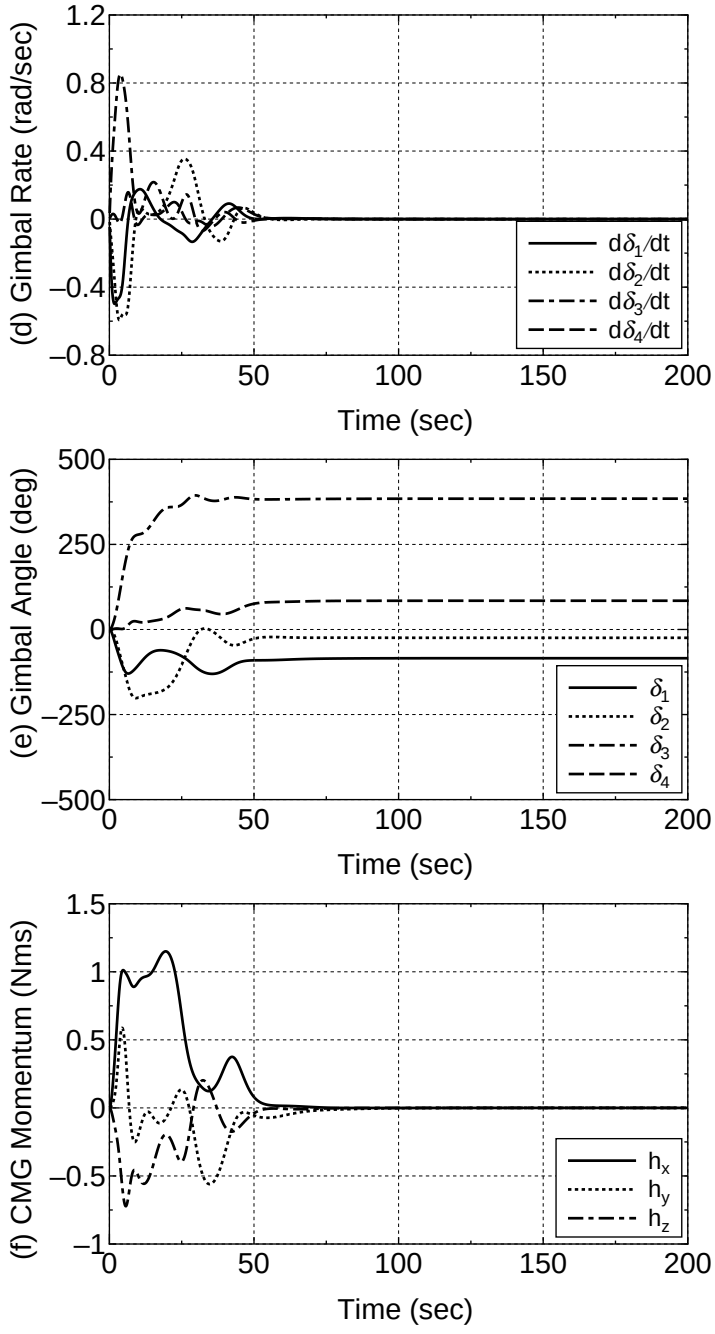

Figure 5.13: Simulation result: **Case 2** (GS controller)

5.4 Conclusion

In this chapter, this thesis is addressed attitude control problems via LPV control theory. First, a pointing control using only two SGCMGs is dealt in Section 5.2. To achieve this pointing control, the author developed a GS controller via LPV control theory. The spacecraft model with SGCMGs was described as an LPV system. Then, a GS controller was designed for this LPV system. The GS controller is effectively worked than the proposed two step strategy in Chapter 4.

The author also dealt the general maneuvers of the spacecraft with four SGCMGs in Section 5.3. The feasibility of the developed GS controller was validated through numerical simulations.

Though the proposed method leaves room for improvements, this thesis proposed a new control method for an ACS using SGCMGs.

Chapter 6

Conclusions

This thesis provided control algorithms for attitude control problems of small satellites using SGCMGs. The SGCMG system has a simple mechanical structure and high torque amplification. The use of SGCMG system can lead to an increase in the pointing accuracy of small satellites.

In this thesis, a cluster of 4-SGCMGs in pyramid type configuration has been studied for fixed-stars tracking attitude control of small satellites. The singularities of the steering logic have been investigated to show the singularity surfaces in three-dimensional angular momentum space. The present method utilizes the singular value decomposition to obtain the singular vector and generates the command gimbal rate that keeps the command torque in the direction orthogonal to the singular direction with maximum gain. The result of the numerical simulation demonstrates the advantage of the proposed method in singularity avoidance over the conventional SR steering law. The SR algorithm simply utilizes an artificially perturbed command torque in order to avoid the singularity, whereas the present method efficiently generates the command torque in the direction orthogonal to the singular direction with a maximum gain to escape from the singular point rapidly.

This thesis also addressed a pointing control using two SGCMGs. The feasible orientations of a spacecraft at rest are possible restrictively due to the angular momentum conservation principle. To solve this problem, the author proposed a control strategy which consists of two steps. The feasibility of the proposed control strategy is validated through numerical simulations. This results are expected to be the countermeasure for a failure in the redundant CMG system (e.g., four CMG cluster).

This thesis also presented attitude control problems via LPV control theory. First, a pointing control using only two SGCMGs is dealt in Section 5.2. To achieve this pointing control, we developed a GS controller via LPV control theory. The spacecraft model with SGCMGs was described as an LPV system. Then, a GS controller was designed for this LPV system. The GS controller is effectively worked than the proposed two step strategy in Chapter 4. The general maneuvers of the spacecraft with four SGCMGs are also dealt in Section 5.3. The feasibility of the developed GS controller was validated through numerical simulations. Though the proposed method leaves room for improvements, this thesis proposed a new control method for an ACS using SGCMGs.

In the present thesis, it has been assumed that the spacecraft model is a rigid body. As future works, an attitude control of a spacecraft with flexible appendage is an important issue that needs to be considered.

The author believes that the results of the present work can contribute to the development of the CMGs which are highly useful attitude control actuators for agile small satellites.

Appendix

A The System Matrices of $A_r(\gamma)$ and $B_r(\gamma)$

The matrices $A_r(\gamma)$ and $B_r(\gamma)$ in Eq. (5.22) can be written as

$$A_r(\gamma) = \begin{bmatrix} 0 & 0 & \frac{2h_w \sin\gamma_1 \cos\gamma_2}{J_x} & 0 & 0 \\ 0 & 0 & \frac{-2h_w \cos\gamma_1 \cos\gamma_2}{J_y} & 0 & 0 \\ \frac{-2h_w \sin\gamma_1 \cos\gamma_2}{J_z} & \frac{2h_w \cos\gamma_1 \cos\gamma_2}{J_z} & 0 & 0 & 0 \\ 0 & 0 & 0 & 0 & 0 \\ \cos\gamma_1 & \sin\gamma_1 & & & \end{bmatrix},$$

$$B_r(\gamma) = \begin{bmatrix} \frac{2h_w \sin\gamma_1 \cos\gamma_2}{J_x} & \frac{2h_w \cos\gamma_1 \sin\gamma_2}{J_x} \\ \frac{-2h_w \cos\gamma_1 \cos\gamma_2}{J_y} & \frac{2h_w \sin\gamma_1 \sin\gamma_2}{J_y} \\ 0 & 0 \\ 1 & 0 \\ 0 & 0 \end{bmatrix}$$

where h_w is the magnitude of the angular momentum of the flywheel, and J_k is the moment of inertia with respect to each body axis $k = x,\ y,\ z$.

B The Coefficient Matrices for Controller Design

For a numerical simulation A, coefficient matrices C, D, and E are given as follows:

$$C = \begin{bmatrix} 30 & 0 & 0 & 0 & 0 & 0 & 0 \\ 0 & 30 & 0 & 0 & 0 & 0 & 0 \\ 0 & 0 & 30 & 0 & 0 & 0 & 0 \\ 0 & 0 & 0 & 0.1 & 0 & 0 & 0 \\ 0 & 0 & 0 & 0 & 0.1 & 0 & 0 \\ 0 & 0 & 0 & 0 & 0 & 1 & 0 \\ 0 & 0 & 0 & 0 & 0 & 0 & 1 \\ 0 & 0 & 0 & 0 & 0 & 0 & 0 \\ 0 & 0 & 0 & 0 & 0 & 0 & 0 \end{bmatrix},$$

$$D = \begin{bmatrix} 0 & 0 \\ 0 & 0 \\ 0 & 0 \\ 0 & 0 \\ 0 & 0 \\ 0 & 0 \\ 0 & 0 \\ 1 & 0 \\ 0 & 1 \end{bmatrix}, \quad E = \begin{bmatrix} 1 & 0 & 0 & 0 \\ 0 & 1 & 0 & 0 \\ 0 & 0 & 1 & 0 \\ 0 & 0 & 0 & 0 \\ 0 & 0 & 0 & 1 \\ 0 & 0 & 0 & 0 \\ 0 & 0 & 0 & 0 \end{bmatrix}$$

For a numerical simulation B, coefficient matrices C, D, and E are given as follows:

$$C = \begin{bmatrix} \sqrt{10^7} & 0 & 0 & 0 & 0 & 0 & 0 & 0 & 0 & 0 \\ 0 & \sqrt{10^7} & 0 & 0 & 0 & 0 & 0 & 0 & 0 & 0 \\ 0 & 0 & \sqrt{10^7} & 0 & 0 & 0 & 0 & 0 & 0 & 0 \\ 0 & 0 & 0 & \sqrt{10^6} & 0 & 0 & 0 & 0 & 0 & 0 \\ 0 & 0 & 0 & 0 & \sqrt{10^6} & 0 & 0 & 0 & 0 & 0 \\ 0 & 0 & 0 & 0 & 0 & \sqrt{10^6} & 0 & 0 & 0 & 0 \\ 0 & 0 & 0 & 0 & 0 & 0 & 1 & 0 & 0 & 0 \\ 0 & 0 & 0 & 0 & 0 & 0 & 0 & 1 & 0 & 0 \\ 0 & 0 & 0 & 0 & 0 & 0 & 0 & 0 & 1 & 0 \\ 0 & 0 & 0 & 0 & 0 & 0 & 0 & 0 & 0 & 1 \\ 0 & 0 & 0 & 0 & 0 & 0 & 0 & 0 & 0 & 0 \\ 0 & 0 & 0 & 0 & 0 & 0 & 0 & 0 & 0 & 0 \\ 0 & 0 & 0 & 0 & 0 & 0 & 0 & 0 & 0 & 0 \\ 0 & 0 & 0 & 0 & 0 & 0 & 0 & 0 & 0 & 0 \end{bmatrix},$$

$$D = \begin{bmatrix} 0 & 0 & 0 & 0 \\ 0 & 0 & 0 & 0 \\ 0 & 0 & 0 & 0 \\ 0 & 0 & 0 & 0 \\ 0 & 0 & 0 & 0 \\ 0 & 0 & 0 & 0 \\ 0 & 0 & 0 & 0 \\ \sqrt{10^7} & 0 & 0 & 0 \\ 0 & \sqrt{10^7} & 0 & 0 \\ 0 & 0 & \sqrt{10^7} & 0 \\ 0 & 0 & 0 & \sqrt{10^7} \end{bmatrix}, \quad E = \begin{bmatrix} 1 & 0 & 0 & 0 & 0 & 0 \\ 0 & 1 & 0 & 0 & 0 & 0 \\ 0 & 0 & 1 & 0 & 0 & 0 \\ 0 & 0 & 0 & 1 & 0 & 0 \\ 0 & 0 & 0 & 0 & 1 & 0 \\ 0 & 0 & 0 & 0 & 0 & 1 \\ 0 & 0 & 0 & 0 & 0 & 0 \\ 0 & 0 & 0 & 0 & 0 & 0 \\ 0 & 0 & 0 & 0 & 0 & 0 \\ 0 & 0 & 0 & 0 & 0 & 0 \end{bmatrix}$$

References

[1] Apkarian, P., Gahinet, P., and Becker, G., " Self-scheduled $\mathcal{H}_\infty$ Control of Linear Parameter-varying Systems: a Design Example, " *Automatica*, vol. 31, no. 9, pp. 1251-1261, 1995.

[2] Bedrossian, N. S., Paradiso, J., Bergmann, E. V., and Rowell, D.," Redundant Single Gimbal Control Moment Gyroscope Singularity Analysis, " *Journal of Guidance, Control, and Dynamics*, vol. 13, no. 6, pp. 1096-1101, 1990.

[3] Creshaw, J., " 2-SPEED, a Single-Gimbal Control Moment Gyro Attitude Control System, " *AIAA Paper 73-895*, 1973.

[4] Gao, R., Kajiwara, H., and Kondo, E., " Depth Control of An Underwater Vehicle Using Linear Parameter-Varying Techniques, " *Proc. of The Twelfth International Offshore and Polar Engineering Conference*, pp. 301-306, Kitakyushu, Japan, 2002.

[5] Han, C., and Pechev, A. N., " Underactuated Satellite Attitude Control with Two Parallel CMGs, " *IEEE International Conference on Control and Automation*, Guangzhou, CHINA, 2007.

[6] Krishnan, H., McClamroch, N. H., and Reyhanoglu, M.," Attitude Stabilization of a Rigid Spacecraft Using Two Momentum Wheel Actuators, " *Journal of Guidance, Control, and Dynamics*, vol. 18, no. 2, pp. 256-263, 1995.

[7] Kurokawa, H., " Constrained Steering Law of Pyramid-Type Control Moment Gyros and Ground Tests, " *Journal of Guidance, Control, and Dynamics*, vol. 20, no. 3, pp. 445-449, 1997.

[8] Kurokawa, H., " A Geometry Study of Single Gimbal Control Moment Gyros - Singularity Problem and Steering Law, " *Technical Report of Mechanical Engineering Laboratory*, Japan, no. 175, 1998.

[9] Lappas, V. J., Oosthuizen, P., Madle, P., Cowie, L. P., Yuksel, G., and Fertin, D., " Design, Analysis and In-orbit Performance of the BILSAT-1 Microsatellite Twin Control Moment Gyroscope Experimental Cluster, " *AIAA Guidance, Navigation, and Control Conference and Exhibit*, Providence, Rhode Island 2004.

[10] Marcos, A., and Balas, G. J., " Development of Linear-Parameter-Varying Models for Aircraft, " *Journal of Guidance, Control, and Dynamics*, vol. 27, no. 2, pp. 218-228, 2004.

[11] Margulies, G., and Aubrun, J. N., " Geometric Theory of Single-Gimbal Control Moment Gyro Systems, " *The Journal of the Astronautical Science*, vol. 26, no. 2, pp. 159-191, 1978.

[12] Marshall, A., and Tsiotras, P., " Spacecraft Angular Velocity Stabilization Using a Single-Gimbal Variable Speed Control Moment Gyro, " *AIAA Paper 03-5654*, 2003.

[13] Morin, P. and Samson, C., " Time-Varying Exponential Stabilization of a Rigid Spacecraft with Two Control Torques, " *IEEE Transactions on Automatic Control*, vol. 42, no. 4, pp. 528-534, 1997.

[14] Nakamura, Y., and Hanafusa, H., " Inverse Kinematic Solutions with Singularity Robustness for Robot Manipulator Control, " *Journal of Dynamic Systems, Measurement, and Control*, vol. 108, Sept., pp. 163-171, 1986.

[15] Oh, H., and Vadali, S.," Feedback Control and Steering Laws for Spacecraft Using Single Gimbal Control Moment Gyro, " *The Journal of the Astronautical Sciences*, vol. 39, no. 2, pp. 183-203, 1991.

[16] Okubo, H., Tani, Y., " Singularity Robust Steering of Redundant Single Gimbal Control Moment Gyros for Small Satellites, " *Proc. of The 8th International Symposium on Artificial Intelligence, Robotics and Automation in Space*, Munich, Germany, 2005.

[17] Paradiso, J. A.," Global Steering of Single Gimballed Control Moment Gyroscopes Using a Directed Search, " *Journal of Guidance, Control, and Dynamics*, vol. 15, no. 5, pp. 1236-1244, 1992.

[18] Shamma, J. S., and Cloutier, J. R., " Gain Scheduled Missile Autopilot Design Using Linear Parameter Varying Transformations, " *Journal of Guidance, Control, and Dynamics*, vol. 16, no. 2, pp. 256-263, 1993.

[19] Shimomura, T., and Kubotani, T., " Gain-Scheduled Control under Common Lyapunov Functions: Conservatism Revisited, " *Proc. of 2005 American Control Conference*, pp. 870-875, Portland, OR, USA, 2005.

[20] Tani, Y., Okubo, H., Tokutake, H., and Azuma, H., " Singularity Robust Control of Redundant Control Moment Gyros for Small Satellites, " *Proc. of The 24th International Symposium on Space Technology and Science 2004-d-42*, Miyazaki, Japan, 2004.

[21] University of Surrey (Surrey Space Centre), SSHP (Small Satellites Home Page), " http://centaur.sstl.co.uk/SSHP/sshp_classify.html "

[22] Vadali, S. R., Oh, H. S., and Walker, S. R., " Preferred Gimbal Angles for Single Gimbal Control Moment Gyros, " *Journal of Guidance, Control, and Dynamics*, vol. 13, no. 6, pp. 1090-1095, 1990.

[23] Wie, B., Bailey, D., and Heiberg, C. J., " Singularity Robust Steering Logic for Redundant Single-Gimbal Control Moment Gyros, " *Journal of Guidance, Control, and Dynamics*, vol. 24, no. 5, pp. 865-872, 2001.

[24] Wie, B., " Singularity Analysis and Visualization for Single-Gimbal Control moment Gyro Systems, " *Journal of Guidance, Control, and Dynamics*, vol. 27, no. 2, pp. 271-282, 2004.

[25] Yamada, K., Takatsuka, N., and Shima, T., " Spacecraft Pointing Control Using a Variable-Speed Control Moment Gyro, " *Proc. of the 26th International Symposium on Space Technology and Science 2008-d-15*, Hamamatsu,Japan, 2008.

[26] Yoon, H., and Tsiotras, P., " Singularity Analysis of Variable-Speed Control Moment Gyros, "*Journal of Guidance, Control, and Dynamics*, vol. 27, no. 3, pp. 374-386, 2004.

[27] Yoon, H., and Tsiotras, P., " Spacecraft Line-of-Sight Control Using a Single Variable-Speed Control Moment Gyro, "*Journal of Guidance, Control, and Dynamics*, vol. 29, no. 6, pp. 1295-1308, 2006.

[28] Yu, Z., Chen, H., and Woo, P., " Gain Scheduled LPV $\mathcal{H}_\infty$ Control Based on LMI Approach for a Robotic Manipulator, " *Journal of Robotic Systems*, vol. 19, no. 12, pp. 585-593, 2002.

List of Publications

No.	Title of the Article	Author(s)	Journal's/Conference's Name, Vol., Pages (Year).	Corresponding Chapter
1	Fixed-Star Tracking Attitude Control of Spacecraft Using Single-Gimbal Control Moment Gyros	S. Kwon Y. Tani H. Okubo T. Shimomura	American Journal of Engineering and Applied Sciences Vol. 3, Issue 1, pp. 865-871 (2010).	Chapter 3
2	Spacecraft Angular Velocity Stabilization Using Two Single-Gimbal Control Moment Gyros	S. Kwon H. Okubo	26th International Symposium on Space Technology and Science, 2008-d-16, CD-ROM, Total 6 pages, (Hamamatsu, Japan, 2008).	Chapter 4
3	Pointing Control of Spacecraft Using Two Single-Gimbal Control Moment Gyros	S. Kwon H. Okubo T. Shimomura	27th International Symposium on Space Technology and Science, 2009-d-51, CD-ROM, Total 6 pages, (Tsukuba, Japan, 2009).	Chapter 4
3′	Pointing Control of Spacecraft Using Two Single-Gimbal Control Moment Gyros	S. Kwon H. Okubo T. Shimomura	Transactions of the Japan Society for Aeronuatical and Space Sciences, Aerospace Technology Japan, (submitted).	Chapter 4
4	Pointing Control of Spacecraft Using Two SGCMGs via LPV Control Theory	S. Kwon T. Shimomura H. Okubo	60th International Astronautical Congress, IAC-09-C1.6.6, CD-ROM, Total 8 pages, (Daejeon, Korea, 2009).	Chapter 5
4′	Pointing Control of Spacecraft Using Two SGCMGs via LPV Control Theory	S. Kwon T. Shimomura H. Okubo	Acta Astronautica, (submitted).	Chapter 5